ACS OMEGA

Open Access

http://pubs.acs.org/journal/acsodf

Review

A Comprehensive Review on Strategies for Enhancing the Performance of Polyanionic-Based Sodium-Ion Battery Cathodes

Anupama Joy, Khusboo Kumari, Fatma Parween, Mst Shubnur Sultana, and Ganesh Chandra Nayak*

Cite This: *ACS Omega* 2024, 9, 22509−22531

Read Online

ACCESS | Metrics & More | Article Recommendations | Supporting Information

ABSTRACT: The significant consumption of fossil fuels and the increasing pollution have spurred the development of energy-storage devices like batteries. Due to their high cost and limited resources, widely used lithium-ion batteries have become unsuitable for large-scale energy production. Sodium is considered to be one of the most promising substitutes for lithium due to its wide availability and similar physiochemical properties. Designing a suitable cathode material for sodium-ion batteries is essential, as the overall electrochemical performance and the cost of battery depend on the cathode material. Among different types of cathode materials, polyanionic material has emerged as a great option due to its higher redox potential, stable crystal structure, and open three-dimensional framework. However, the poor electronic and ionic conductivity limits their applicability. This review briefly discusses the strategies to deal with the challenges of transition-metal oxides and Prussian blue analogue, recent developments in polyanionic compounds, and strategies to improve electrochemical performance of polyanionic material by nanostructuring, surface coating, morphology control, and heteroatom doping, which is expected to accelerate the future design of sodium-ion battery cathodes.

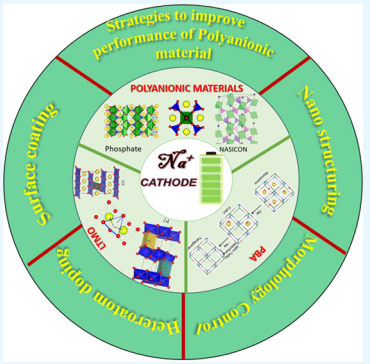

1. INTRODUCTION

The whooping energy demands and environmental concerns regarding the emission of toxic gases during the consumption of fossil fuels make nonrenewable energy sources unsuitable for future energy needs.[1] The search for an efficient, clean, and sustainable source of energy paved the way for the growth of renewable energy sources such as tidal energy, solar energy, and wind energy. However, their intermittent energy supply due the variable weather conditions diminishes their reliability on the global market.[2,3] Hence suitable electrochemical energy storage devices are required for the production of electricity from renewable energy sources. Batteries are becoming popular among electrochemical storage devices because of their higher energy efficiency.[4]

Even though the research on sodium-ion batteries (SIB) started parallel with lithium-ion batteries (LIB) in 1980, LIBs dominated the industry due to their higher energy efficiency and long life span which made LIB an ideal energy storage device after its commercialization in 1991 by Sony Corporation with carbon as anode and $LiCoO_2$ as cathode.[5] Mainly there are four main components in an LIB system—cathode, anode, current collector, and electrolyte. Cobalt and nickel-based transition-metal oxides are generally used as cathode materials, graphite is used as anode, and copper serves as a current collector. The demand for LIB has increased with the fast-growing electronic grid appliances and electric vehicle industry. However, the raw materials of LIBs, mainly lithium, cobalt, and copper, are rare elements where the relative abundance of lithium is limited to 20 ppm and its uneven distribution around the world has raised concern about the price and its long-term availability.[6,7] A steep increase in the price of $LiCoO_2$ can be seen in the beginning of this century due to the widespread use of LIBs.[8] Generation of heat during a charging−discharging cycle due to the electrochemical reaction increases the battery temperature, and a failure in the management of heat can cause combustion or even explosion, which raises safety concerns in LIBs.[9] According to P. Rüetschi "three E" determines the success of a battery, i.e., energy, economics, and environment. Considering the abundance, cost, and safety issues conventional LIBs have become less suitable for the vast future energy needs.[10] These concerns motivated the researchers to find suitable alternative energy storage devices for LIBs (Figure 1).

In comparison to lithium, sodium resources are limitless, as sodium is one of the most prevalent elements found in the earth's crust. It is the smallest alkali metal next to Lithium, and its comparable physical and chemical properties with Li, have made SIBs an ideal substitute for LIBs. SIB cathodes rely on abundant iron and manganese, rather than scarce nickel and cobalt, for its electrode material. And unlike geologically constrained lithium resources, sodium is evenly distributed all over the world making it easily available. Another advantage of SIB is that sodium is free from alloying reaction with aluminum, so the cheaper aluminum

Received: March 20, 2024
Revised: April 18, 2024
Accepted: April 26, 2024
Published: May 13, 2024

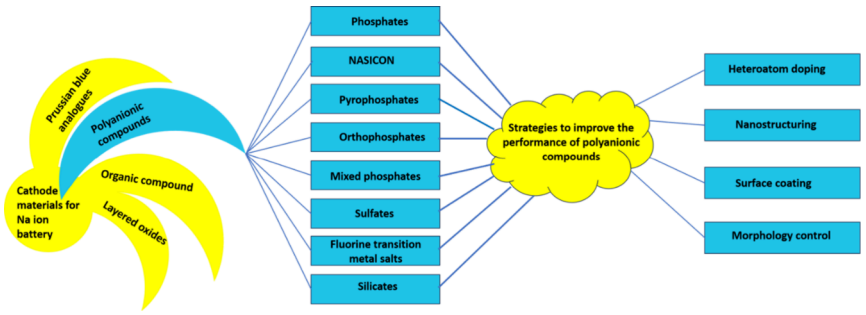

Figure 1. Schematic illustration of types of cathode materials along with the strategies to improve their performance.

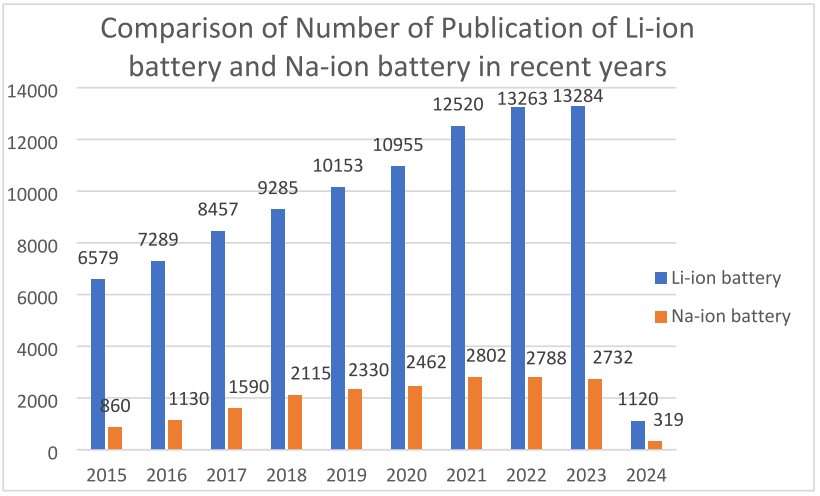

Figure 2. Comparison of number of publications of Li-ion battery and Na-ion battery in recent years. Source: Web of Science. Data until 2024 February.

serves as a current collector rather than copper, which further reduces the cost. The use of same current collector makes it easy to recycle and also enables SIBs to be stored at 0 V.[11] This ability of SIBs to be transported in short-circuit stage compared to LIBs, which is stored and transported in 20−40% charge state to avoid the dissolution of copper, makes it safer. Further, Na^+ ion being larger in size has a low charge density as compared to the Li^+ ion and thus has low desolvation energy. This facilitates higher mobility of Na^+ ions and makes it easier for Na^+ to move between electrode and electrolyte.[6] Therefore, the faster sodium transport kinetics and easier charge transfer has led to higher rate capability even though it suffers from less polarizing energy.[12] Also, the self-heating temperature for LIBs (165 °C) is less than that of SIBs (260 °C) making SIBs thermally more stable than LIBs.[11] The research interest in the field of Na-ion batteries has increased in recent years due to its wide availability and low cost. A comparison bar plot which shows the number of publications in Li-ion battery and Na-ion battery is given in Figure 2. Threefold increase in number of publications can be observed for Na-ion battery from 2015 to 2023, whereas only two times increase is observed for Li-ion battery. Increasing cost and rare lithium resources make LIBs unsuitable for large-scale energy storage. SIBs are suitable for storage grid appliances where cost and safety are more considered than energy density. A comparison of the properties of Na and Li is given in the Table 1.

SIBs suffer from a lower specific capacity than the LIBs counterparts because of their lower reduction potential and the larger size of Na. However, they have an upper hand over safety, cost effectiveness, and abundance, which make SIBs worthwhile exploring. For large-scale grid storage, cost and longevity are considered more than energy and power density.

Table 1. Comparison of the Properties of Na and Li[13−15]

	Na	Li
Material abundance (ppm)	23,600	20
Shannon's ionic radii (Å)	1.02	0.76
Relative atomic mass	6.94	23.00
***E*° (vs SHE) (V)**	−2.71	−3.04
Melting point (°C)	97.7	180.5
Desolvation energy in PC	157.3 kJ mol^{-1}	218.0 kJ mol^{-1}
Self-heating temperature	260 °C	165 °C
Price	∼0.3$	∼6$
Coordination preference	octahedral and prismatic	octahedral and tetrahedral
Distribution	Everywhere	70% in South America

SIBs work in a similar "rocking chair" mechanism as LIBs as the sodium ions shuttle between the two electrodes because of the voltage generated across cathode and anode. A sodium ion battery consist of a positive electrode-cathode, negative electrode-anode, electrolyte, separator, and current collector. Sodium ions shuttle between cathode and anode during charging and discharging. Initially, SIBs are in a discharged state. The positive electrode contains the transferrable sodium ion, and the anode will be sodium-free. At the time of charging, oxidation occurs at the cathode, and sodium ions deintercalate

https://doi.org/10.1021/acsomega.4c02709
ACS Omega 2024, 9, 22509−22531

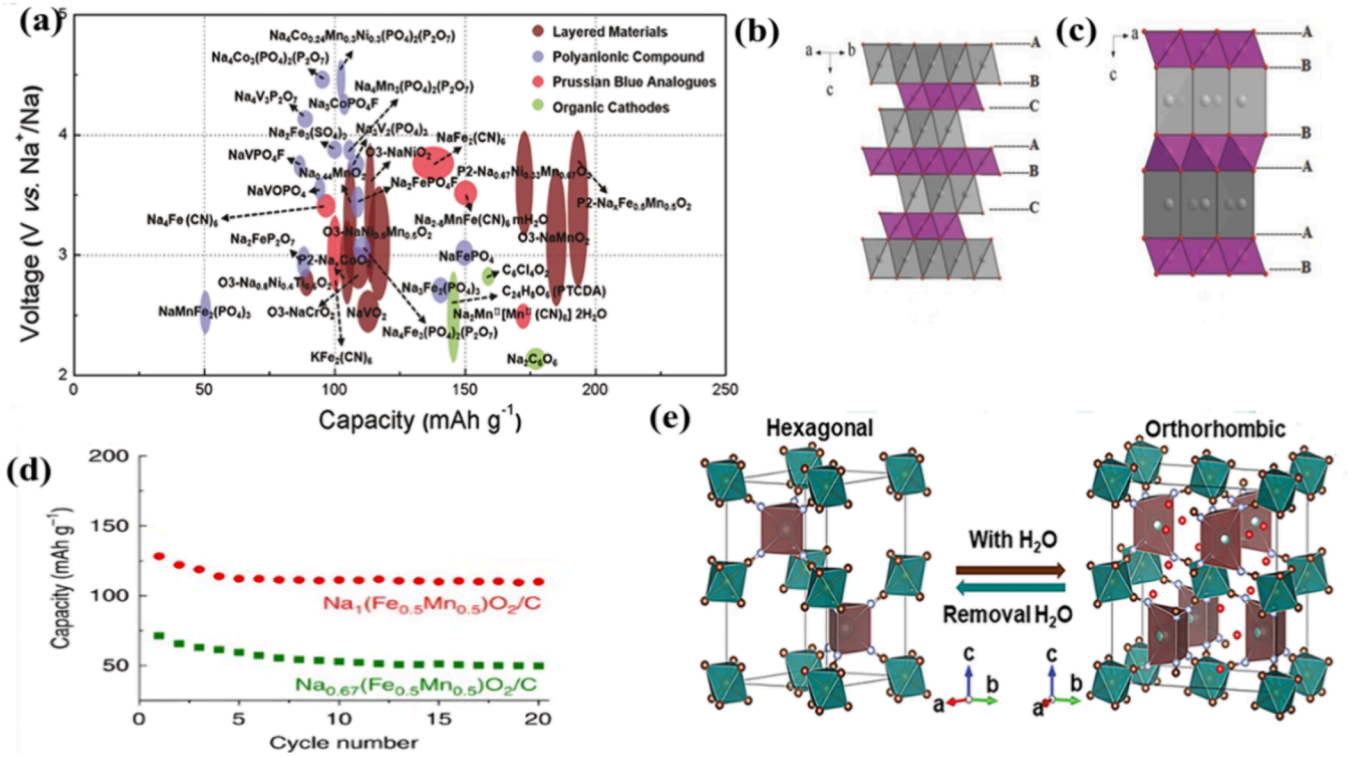

Figure 3. (a) Voltage-Capacity plot of different cathode materials. Reprinted with permission from ref 50, copyright 2016, Wiley.[50] Structural pattern of (b) O3-layered transition metal oxide and (c) P2-layered transition metal oxide. Reprinted with permission from ref 51, copyright 2015, Wiley.[51] (d) Capacity retention of P2−$Na_{0.67}[Fe_{0.5}Mn_{0.5}]O_2$ and P'2-$Na[Fe_{0.5}Mn_{0.5}]O_2$. Reprinted with permission from ref 52, copyright 2016, Nature Communications.[52] (e) Structural changes occurring in PBAs. Reprinted with permission from ref 53, copyright 2022, Wiley.[53]

from the cathode material at a potential around 3.0 V versus Na^+/Na and get into the anode around or lower than 1 V by passing the separator and the electrolyte. To compensate the positive charges of the sodium ions, electrons are transported across the external circuit, i.e., from cathode to anode. During discharging, the circuit is connected to a load, Na^+ ions insert into cathode from electrochemically oxidized anode, and the electrons also transferred from anode to cathode through an external circuit; thus, they reach the initial discharged state. A suitable cathode material which possesses sufficient sodium content, having large interstitial spaces to host bigger Na^+ ion, structurally stable during charging and discharging, and sufficient ionic and electronic conductivity is needed for the commercialization of high power and energy-dense SIBs.[16]

Cathodes are the most important components of SIBs, which have a direct effect on the specific capacity, cycling life, and the operating voltage, and they carry one-third fraction of the battery. It is still a challenge to the research community to find suitable Na host material with a comparable energy density and working potential as Li analogues. After the successful commercialization of $LiCoO_2$ as a cathode material for LIBs, sodim insertion characteristics of Na_xCoO_2 were also studied, and it is found that $LiCoO_2$ has a specific capacity of 402 Wh kg^{-1} when graphite is used as anode material, but the similar P2−$Na_{0.67}CoO_2$ has only reached up to 251 Wh kg^{-1}.[17,18] After realizing cathodes for sodium ion battery cannot be duplicated from the Li analogues, development of various sodium host materials using a large number of transition metals and studies regarding the sodium de/intercalation mechanism have been done for the design of better materials.

Layered transition-metal oxides and polyanionic materials are two main categories of cathode materials for sodium ion batteries. Even though layered transition-metal oxides exhibit high energy density, they suffer from sluggish kinetics, and large volume change and complex phase transitions during charging and discharging reduces the cycling life of battery. Safety issues caused by the release of oxygen are another concern of layered transition-metal oxides. Layered transition metal oxides are highly sensitive to moisture. Structural changes and the formation of electrically insulating surface resulting from the reaction with H_2O and CO_2 degrades the electrochemical properties.[19] Alternatively, polyanionic materials exhibit a great diversity in their structures, especially in polyanions where Na^+ extracting voltage can be tuned by an inductive effect, which is used to design high-voltage electrode material. Voltage-capacity plots of electrode materials for a Na-ion battery are shown in Figure 3(a). The good structural integrity and open framework of polyanionic materials provide a good cycling life. This characteristics provides long-term stability when compared to layered transition metal oxides, making polyanionic materials, a promising electrode material for sodium ion battery. In terms of safety, polyanionic materials have good thermal stability due to the strong covalent bond of oxygen atoms with the nonmetal and with the transition metal.[20] But the high molecular weight of the polyanionic compounds leads to lower specific capacity, resulting in a lower energy density. Polyanionic compounds exhibit low electronic conductivity, especially in the NASICON materials, which affects their electrochemical performance. By using a suitable surface coating, heteroatom doping, modifying the morphology, and nano structuring can alleviate this issue.[21]

The higher thermal stability of the polyanionic compounds, particularly for phosphates due to the P−O bond, are promising for mid-range electric vehicles (EVs) and stationary energy storage.[22] But these compounds lag behind in energy and power

https://doi.org/10.1021/acsomega.4c02709
ACS Omega 2024, 9, 22509−22531

density when compared to layered transition metal oxides, and also the polyanionic groups can render the transport of electrons, which results in the poor capacity and performance of the materials. This review systematically deals with different ways of improving the electronic conductivity of the polyanionic materials, which is very essential for its better performance.[23] This review provides a brief introduction about layered oxides and Prussian blue analogues along with the challenges and the methodologies to improve their performance and discusses recent developments in the field of polyanionic compounds, challenges faced by the material as sodium host, and the strategies to improve their electrochemical performance. Even though there are several papers regarding polyanionic compounds, a review which comprehensively discusses about the different methods for improving the performance of the polyanionic compound is still lacking. Recently, Chunliu Xu et al. published review article which deals with V-based, Fe-based, and Mn-based polyanionic compounds toward high energy density and long cycle life, but the different ways to improve the electronic conductivity, which is a major limiting factor for the decrement in the performance of electrochemical performance, is not addressed.[24] Jin et al.,[25] Zhao et al.,[26] and Barpanda et al.[27] have discussed different kinds of polyanionic materials, their characterization techniques, and the electrochemical performance, but they lack in explaining different strategies to improve the performance. Ling et al.[28] have discussed about electronic properties, different synthesis methods, and ways to improve the electronic conductivity, but the discussion is limited to phosphate-based polyanionic materials. Here we include an introduction to different types of cathode materials, a detailed description about the different kinds of polyanionic materials, and the ways to alleviate the main challenges caused by the material. It is anticipated that this review will be beneficial in developing new polyanionic materials with enhanced electrochemical performance.

1.1. Layered Transition-Metal Oxide. Layered transition-metal oxides have a generic chemical formula of Na_xTMO_{2+y}, where TM stands for transition metal (Mn, Fe, V, Cr, Zn, Ru) and the Na^+ ions are located in between the edge-sharing TMO_6 octahedral sheets.[29] Structurally, layered transition metal oxides are classified mainly into O3 and P2 by Delmas et al.; besides that, O2 and P3 are also present, where P and O correspond to the trigonal prismatic and octahedral sites of sodium ions and 2 and 3 represent numbers of different transition metal oxide layers.[30] O3 is composed of layers that are packed in an ABCABC pattern (Figure 3(b)), with one edge and one face shared by all the sodium, and sodium content is between 0.7 and 1. P2 compounds have a sodium content of about 7, exhibit an ABBA transition metal oxide layer stacking pattern, and share all of the sodium either completely on the edge or completely on the face (Figure 3(c)). Oxide layer stacking in the P3 phase, which occurs when $x \approx 0.5$, displays the ABBCCA pattern, and all of Na share one face and three edges with three MO_6 octahedra.[31] Specific energy and the cyclic life of the material is significantly impacted by the structure of the oxides due to the difference in sodium content, ion diffusion rate, and the difference in phase transitions during intercalation and deintercalation of sodium ions.[31] Even though the sodium content, reversible capacity, and ion diffusion are higher for O3 compounds, it suffers from lower cycling stability due to the complex phase transition that occurs during the charging and discharging process (O3 → O′3 → P3 → P′3 → P3″) for $NaNi_{0.5}Mn_{0.5}O_2$, while the P2 shows P2 → O2 transformation.[32] The multiple phase transitions in SIBs compared to LIBs are mainly attributed to the larger size of sodium, elongated Na−O bonds, and the ordering arrangement between Na and vacancies created at various Na contents.[29] During charging, sodium from the cathode transfers to the anode, resulting in the decrease of sodium content in the cathode, which further proceeds to gliding of the metal oxide layer due to the repulsion between oxygen atoms leading to the successive phase transitions.[33] The limited phase transitions in the P2 phase lead to the comparatively higher structural stability in P2, which contributes to the good cycling stability and the higher rate capability. Suppression of phase transition by limiting the cutoff voltage and substituting the transition metal ions by electrochemically inactive and active elements such as Al,[34] Mg,[35] Sb,[36] Zn,[13] Cu,[37] and Fe[38] are explored as they improve the electrochemical performance of layered oxides.[39] Even though limiting the cutoff can reduce the capacity, a stable cycle life can be obtained which is due to the enhanced structural stability of the material.[40] Sodium ion extraction during the electrochemical cycling leads to the gliding of transition metal layers, which eventually changes the symmetry of vacant sites. Generally, a P2 phase transforms to O2 phase due to the gliding of TMO_6 octahedra when a certain amount sodium ion is extracted. This kind of phase transition is responsible for the capacity fading.[41,35] Doping the TM sites with ions having similar radii like Mg, Al, and Zn into the cathode structure changes the local environment, which is found to improve the cyclic stability.[18] From the compounds $Na_{0.67}Ni_{0.33-x}Mg_xMn_{0.67}O_2$,[42] $Na_{0.5}Mn_{0.5-x}Al_xCo_{0.5}O_2$,[34] and $Na_{0.66}Ni_{0.33-x}Zn_xMn_{0.67}O_2$,[43] it is understood that the smaller bond length of the dopant with the oxygen compared to the TM-O bond will reduce the slab thickness of TMO_6. The reduced thickness of the TM layers will increase the *d*-spacing of the Na layer, which in turn results in improved diffusion kinetics of sodium ion during (de)sodiation. The stronger bond of dopant with oxygen increases the overall structural stability of the material. The presence of redox-inactive ions as dopants allows more sodium ions to stay in their sites during charging-discharging to stabilize the overall charge balance. Thus, phase transitions such as P2−O2 are inhibited. Even though limiting the cutoff can reduce the capacity, a stable life cycle can be obtained which is due to the structural stability of the material.[40]

Lower specific energy because of the limited sodium content is another challenge faced by the layered transition metal oxide. Studies have shown that adding sodium sacrificially to the sodium-deficient transition metal oxide can improve the reversible capacity to a large extent. Biao Zhang et al. introduced Na_3P salt to the P2−$Na_{0.67}[Fe_{0.5}Mn_{0.5}]O_2$ and obtained P′2-$Na[Fe_{0.5}Mn_{0.5}]O_2$ in which reversible capacity is increased by 20%. From Figure 3(d) it is observed that reversible capacity has been increased from 71 to 155 mA h g^{-1} by the introduction of a sacrificial sodium source (Na_3P) without any sacrifice in capacity retention. However, the handling of Na_3P salt in the atmospheric air is difficult due to humidity issues.[44] Armand et al. successfully obtained 60% enhancement in reversible capacity by the introduction of 10% Na_3N as a sodium reservoir to P2−$Na_{0.67}[Fe_{0.5}Mn_{0.5}]O_2$. The generation of N_2 gas during oxidation by electrochemical decomposition can hamper battery performance.[45] Further, triggering an oxygen redox reaction in the lattice by mainly substituting lithium is also an effective strategy to improve the storage capacity of the oxides. This can provide a capacity even higher than theoretical capacities, but it suffers from structural degradation due to the oxygen loss from the

https://doi.org/10.1021/acsomega.4c02709
ACS Omega 2024, 9, 22509−22531

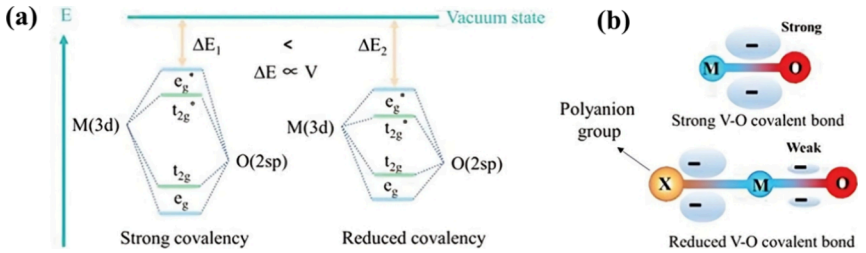

Figure 4. Schematic illustarion of (a) changes in molecular orbitals and (b) covalancy of M-O bond. Reprinted with permission from ref 20, copyright 2020, Wiley.[20]

lattice.[46,47] Chen et al. synthesized P2-type $Na_{0.72}[Li_{0.24}Mn_{0.76}]O_2$ which gives a reversible capacity of 270 mA h g^{-1} and energy density of 700 W h kg^{-1} in the range of 1.5 and 4.5 V.[48]

Sodium transition metal oxides shows lower air stability compared to the Li counterparts due to their lower redox potentials; thus, the atmospheric exposure can deteriorate the performance of material. Reaction with H_2O and CO_2 leads to the formation of Na_2CO_3 and NaOH; this increases the rate of sodium extraction from the lattice. A side reaction occurring at the electrode−electrolyte interface and decomposition of the electrolyte leads to the deposition of the side reactants at the electrode surface, will lower the ionic-electronic conductivity, and lead to the corrosion of electrode material. Hence a protective surface oxide with an oxide layer such as Al_2O_3, MgO, $NaPO_3$ prevents the active surface from direct contact with air, and the electrolyte thus improves the electrochemical performance of the battery.[47,49]

1.2. Prussian Blue Analogues. The chemical formula of Prussian blue analogues (PBAs) can be indicated as $A_xM_1M_2(CN)_6$ where A can be Li^+, Na^+, K^+, or NH_4^+, M_2 is generally occupied by Fe, which is coordinated to low-spin carbon, and M_1 corresponds to transition metal including Mn, Ni, and Co which are coordinated to the high-spin nitrogen of the cyanide group. PBAs are reported by Goodenough's group, and their crystal structure is dictated by the concentration of alkali ions as well as the amount of trapped water; based on this three distinct types of polymorphic structures such as monoclinic, cubic, and rhombohedral are found. Hydrated $Na_{2-\delta}Mn[Fe(CN)_6]$ exhibits a monoclinic structure. Whereas its dehydrated framework shows rhombohedral structure. The alkali-rich framework shows monoclinic configuration, whereas, alkali-deficient one has a cubic framework. The structural change of PBA from hexagonal to orthorhombic with the effect of water is shown in Figure 3(e). Intermediate structural forms are encountered during sodium intercalation and deintercalation.[54]

Generally, the electrochemical performance of the PBA is largely affected by the water content, phase purity, defects, and crystallinity. It is difficult for the PBAs to reach the ideal electrochemical performance due to the $Fe(CN)_6$ vacancy and the coordinated water in the lattice as it distorts the crystal structure, promotes the organic electrolyte decomposition, fastens the side reaction with the electrolyte, and decreases the ion/electron conductivity. Moreover, the positively charged vacancies lower the sodium ion uptake, which lowers the specific capacity.[55,56] Three different kinds of water molecules are present in PBAs, namely, absorbed water, which is comparatively easy to remove by a simple heating procedure below 120 °C, and interstitial and coordinated water, which are difficult to remove due to the physiochemical bonding with the framework. Increasing sodium content during synthesis and prefilling the vacancies can reduce the uptake of water molecules.[57,58] A commonly used hydrothermal and coprecipitation synthesis process of PBAs leads to imperfect crystal growth, thus leading to the formation of a large number of vacancies. Tuning the synthesis process is an effective strategy to produce nanomicro-sized PBAs, with fewer defects, thus improving the specificity of the electrode.[59] The cyclic stability of the PBAs is lowered by the structural degradation that occurs due to the defects in the framework and also by the dissolution of the transition metal ion, which can reduce by a proper surface coating to an extent. Safety concerns regarding the release of cyanide under strong acidic conditions and high temperatures is unignorable. The proper treatment of chemical waste with excess oxidizing agent to fully oxidize cyanide to nontoxic products is being considered.[60]

2. POLYANIONIC COMPOUNDS

Polyanion-type electrode materials are compound that contains a series of tetrahedron anion units $(XO_4)^{n-}$ or their derivatives $(X_mO_{3m}+1)^{n-}$ (X = S, P, Si, As, Mo, or W) with strong covalent-bonded MO_x polyhedra (M represents a transition metal). Due to strong covalently bonded oxygen with the transition metal M and the nonmetal X, they show higher thermal stability compared to other cathode materials, which makes them popular where safety is a concern.[61] Also their minor structural changes during their insertion and deinsertion of sodium ions due to the robust 3D structure is another advantage. Polyanionic materials generally show lower gravimetric densities due to their heavier polyanoinic groups.

The higher redox potential of the polyanionic compounds can be explained with molecular orbital theory. Interactions among the 3d orbital of a transition metal and the 2sp orbital of oxygen (M-O) causes the energy splitting of molecular orbitals into bonding and antibonding orbitals. A highly covalent M-O bond will lead to larger spillting which in turn will decrease the energy difference (ΔE) between the antibonding orbitals and the Fermi level of sodium (vacuum state), thus reducing the voltage as ΔE proportional to the redox potential of the metals. When an electronegative polyanionic group is introduced to the framework, the M-X bond weakens the M-O bond, as it increases the electron density on the transition metal; thus, the antibonding orbitals rise to a lower extent, which raises the redox potential of the transition metal (Figure 4).[23,62]

2.1. Phosphates. After the successful commercilization of $LiFePO_4$,[63] the sodium analogue $NaFePO_4$ was explored as a cathode material for SIB cathodes. $NaFePO_4$ was noticed to have two different phases olivine and maricite where both of the lattices have been formed by the slighty distorted octahedral FeO_6 and the tetrahedral PO_4. Both of the crystal structures belong to the *Pmna* space group where the maricite phase consists of edge-shared FeO_6 units that are linked with PO_4 with

https://doi.org/10.1021/acsomega.4c02709
ACS Omega 2024, 9, 22509−22531

no Na^+ diffusion channels, thus being considered as electrochmically inert, whereas in the olivine phase neighboring FeO_6 units are corner-shared with PO_4, giving rise to a 1D catonic channel along the *b*-axis.[64,65] Olivine and maricite sites differ in the occupation sites of Na^+ and Fe^{2+}; in olivine, Na^+ occupies the M1 sites and Fe^{2+} in the M2 sites, whereas in the case of marcite Na^+ occupies the M2 sites and the Fe^{2+}occupies M1 sites as shown in Figure 5(a,b). Due to the long distance between the

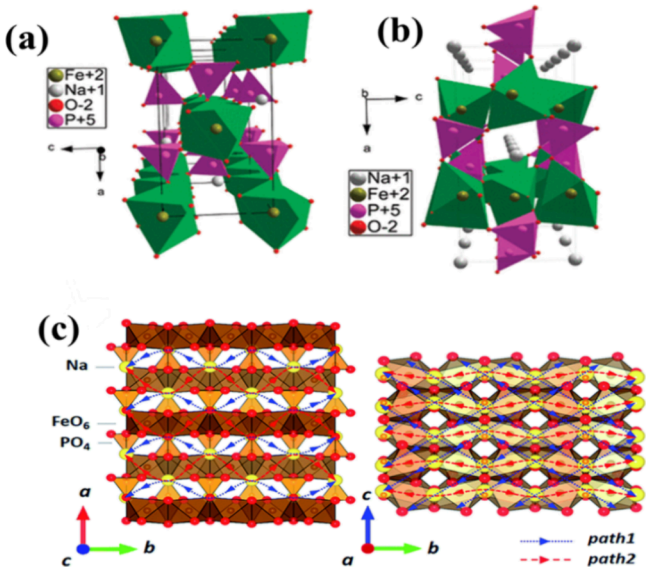

Figure 5. Structure of (a) maricite $NaFePO_4$ and (b) olivine $NaFePO_4$. Reprinted with permission from ref 65, copyright 2010, American Chemical Society.[65] (c) Na diffusion channel in maricite $NaFePO_4$. Reprinted with permission from ref 73, copyright 2015, Royal Society of Chemistry.[73]

M2 sites, alkali-ion hopping is not possible in maricite. Kim et al. through quantum mechanics (QM) and density functional theory (DFT) calculations found that Na diffusion in $Na_{1-x}FePO_4$ ($x \approx 0$) can occur through two possible ways: Path 1 is along the *bc* plane, and path 2 is along the *b* direction as shown in Figure 5(c,d).[66] Olivine $NaFePO_4$ has been widely accepted due to the excellent theoretical capacity and energy density of 154 mA h g^{-1} and 446 W h kg^{-1}, respectively, and an operating potential of 2.9 V (vs Na^+/Na) based on Fe^{3+}/Fe^{2+} single redox couple.[67] Na ions and the Fe ions accommodate crystallographically different octahedral sites as they have different charges and size and the P atoms found at 1/8th of tetrahedral sites within the hexagonal close-packed (hcp) oxygen framework. A direct high-temperature synthesis route produces a thermodynamically stable maricite phase rather than olivine; thus, it generally requires complicated cation exchange from $LiFePO_4$.[68,69]

$$LiFePO_4 + NO_2BF_4 \rightarrow FePO_4 + LiBF_4 + NO_2$$

(de-lithiation)

$$FePO_4 + 3/2NaI \rightarrow NaFePO_4 + 1/2NaI_3 \text{ (sodiation)}$$

The stability studies of maricite and olivine phases have been reported by P. Moreau and group.[65] A sodium exchange reaction in olivine $NaFePO_4$ is a two-step process separated by a voltage drop having intermediate $Na_{0.7}FePO_4$ stage which is related to the Na^+ ordering in the lattice framework.[70] The practical capacity of the olivine phase lags behind the theoretical capacity due to the high charge transfer kinetics and low ionic conductivity, and this can be minimized through proper surface coating and optimizing the morphology. Ghulam Ali et al. developed olivine $NaFePO_4$ modified with polythiophene having discharge capacity of 142 mA h g^{-1} with a cyclic stability of 94% over 100 cycles (Figure 6(a)). The material exhibits excellent electrochemical performance due to the electrical conduction generated by the polythiophene layer.[71]

Doping another redox-active metal with olivine $NaFePO_4$ is an efficient method to enhance the voltage of the material. Partial substitution of Fe by Mn was also explored in the olivine phase, and it was found that 10−20% of Mn substitution can enhance the capacity by >15% through a kinetically produced intermediate phase that reduces the volume disparity between the fully sodiated and desodiated phases.[72]

For the first time, Kim et al. reported 50 nm particle sized maricite $NaFePO_4$ which shows a capacity of 142 mA h g^{-1} at 0.05 C; here, the sodium ion diffusion occurs through the two

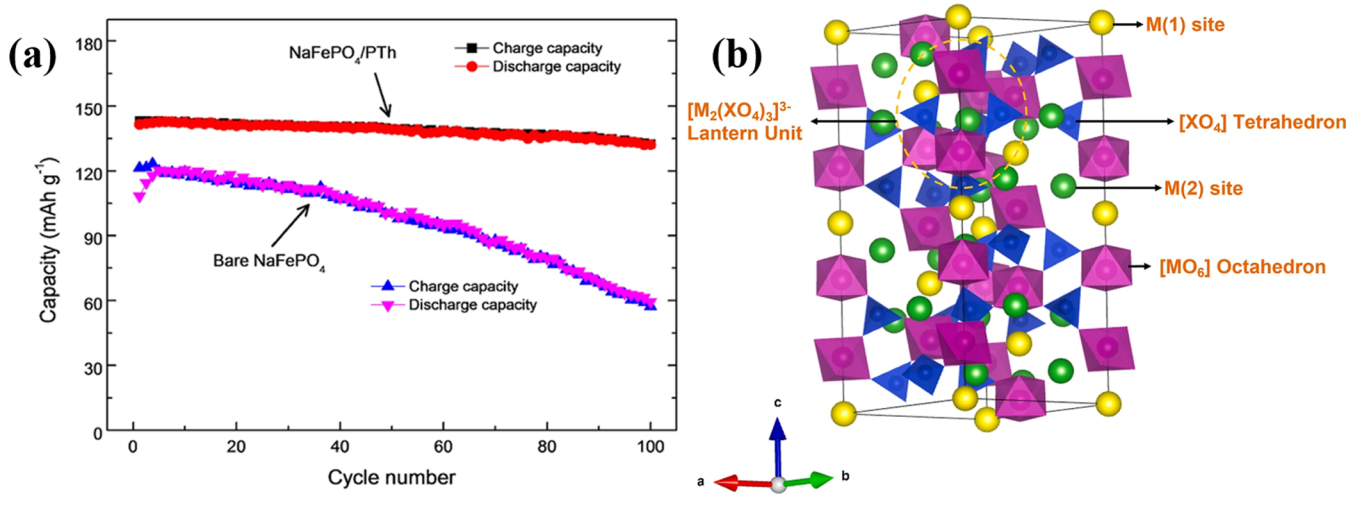

Figure 6. (a) Capacity retention of bare $NaFePO_4$ and PTh-coated $NaFePO_4$. Reprinted with permission from ref 71, copyright 2016, American Chemical Society.[71] (b) NASICON crystal structure having rhombohedral symmetry. The lantern unit is highlighted by the dash line. Reprinted with permission from ref 78, copyright 2023, Elsevier.[78]

https://doi.org/10.1021/acsomega.4c02709
ACS Omega 2024, 9, 22509−22531

pathways—path 1 in the *bc* plane and path 2 along the *b* direction—as shown in Figure 5(c).

Following the initial desodiation, maricite $NaFePO_4$ changes into amorphous $FePO_4$, which has lower barriers to sodium ion hopping. The electrochemical characteristics of amorphous $FePO_4$ are used to determine subsequent charging and discharging.[73] Reducing the size of the marcite phase to nanoscale is an effective strategy to mitigate the poor kinetics due the large mismatch between the maricite and amorphous phases (17.58% in unit volume), and the lower electronic conductivity of the maricite phase is another drawback besides the restricted ion mobility. A hybrid of maricite $NaFePO_4$/C/graphene was synthesized by Rahman et al. with $NaFePO_4$ particle sizes varying from 40 to 150 nm. It demonstrated a rate performance of 51 mA h g^{-1} at 5 C and a 98% cycling life after 300 cycles. Nanosizing of the material leads to increased reactive sites, and also it shortens the ion transport distance. Yong-chang Liu et al. synthesized binder-free nanosized maricite $NaFePO_4$ having 1.6 nm size coated with porous N-doped carbon nanofibers by an electrospinning method which has a reversible capacity of 145 mA h g^{-1} at 0.2 C, high rate capability of 61 mA h g^{-1} at 50 °C, and capacity retention of 89% over 6300 cycles.[74]

The $NaMnPO_4$ material exhibits both olivine and maricite phases, with the olivine phase facilitating Na^+ diffusion through edge-sharing octahedra along the *b*-axis, while Na^+ mobility is hindered in the thermally stable maricite structure. Despite various synthesis methods like ion exchange, phosphate-format precursor, and topotactic molten salt reaction being employed for optimization, there remains a limited amount of research on the underlying mechanism of $NaMnPO_4$. To gain a comprehensive understanding of its electrochemical properties, additional strategies, such as carbon coating, is necessary.[75]

2.2. NASICON. NASICON (Sodium superionic conductor) structured materials $Na_xM_2(PO_4)_3$ (M = V, Ti; x = 1,2,3) are a class of materials well-known for its higher ion diffusion rates and stable 3D framework which in turn provides good cyclic stability and satisfactory rate capability compared to the olivine type of polyanionic compounds.[76] They usually exhibit a rhombohedral structure with $R\bar{3}c$ space group where each MO_6 octahedron interlinked to three XO_4 tetrahedral units with corners to establish $[M_2(PO_4)_3]^{3-}$ and forms a lantern structure which gives rise to a three-dimensional open framework with ample Na^+ diffusion paths (Figure 6(b)). Two kinds of interstitial sites (Na1 and Na2) are formed in the framework for sodium occupation in the crystal structure. These interstitial sites were connected with the conduction pathways resulting in the fast kinetics of Na ions. Na1 occupies $2Na^+$ ions and Na2 occupies $6Na^+$ ions. Na^+ ions from Na2 sites are extracted more readily than from Na1 sites due to the weak bonding energy. The chemical tunability of cation and anion offers great opportunities for material engineering.[77]

Among the reported single and binary types of transition metal, the type $Na_3V_2(PO_4)_3$ having a specific capacity and energy density of 117 mA h g^{-1} and 392 W h kg^{-1} is considered as the most promising cathode candidate due to the high cyclic stability and the working potential of 3.3−3.4 V.[79] The recent structural studies of $Na_3V_2(PO_4)_3$ show that it cannot be assigned to the typical $R\bar{3}c$ at room temperature as it shows four distinct crystal structures (a, b, b′, g) from −30 to 225 °C. At lower temperature a phase with long-range Na^+ ordering belonging to the $C2/c$ space group is formed. In two intermediate-temperature β and β' monoclinic phases are incommensurate modulated structures. At temperature above 180 °C rhombohedral form γ ($R\bar{3}c$) appears where the sodium ions are fully distributed in the interstitial sites.[80] Besides this material has two different voltage plateaus at around 3.3 and 1.6 V which make it suitable for cathode and anode material simultaneously. However, the electrochemical performance of the $Na_3V_2(PO4)_3$ still needed to be improved in terms of reversibility and cyclability. The absence of direct M-OM electronic delocalization and the presence of polyanionic groups lead to poor electronic conductivity, which is also a challenge to deal with, cationic substitution, carbon coating, and supporting are ways to fasten the reaction kinetics and improve the performance.

For carbon coating other than organics such as glucose, sucrose, citric acid, oxalic acid, reduced graphene oxide (rGO), and carbon nanotubes, polymers are also employed. In addition Yanping Zhou et al. reported 3D carbon foams consisting of mesoporous nanofibers through the assembly of recombinant elastin-like polypeptides (ELP16) proteins, which shown superior rate capability of 73 mA h g^{-1} at 100 °C. This is because the transport characteristics have improved due to the unique pore-like morphology which provided quick transport pathways for the sodium ions. In addition improved surface area of electrodes achieved through the coating permits larger contact area with the electrolytes.[81] Heteroatom doping on the single carbon layer is also explored as the dopant can increase the interlayer spacing of the carbon layers, which can ease the intercalation and deintercalation of Na^+ ions in addition to creating active defects which improves the electron transfer. Wei Li et al. made a composite of highly porous $Na_3V_2(PO_4)_3$ with sulfur-doped carbon which shows a rate performance of 116.5 mA h g^{-1} at 1C and a capacity retention of 91% after 2500 cycles.[82,83]

2.3. Pyrophosphates. Phosphorus oxyanions that contain two phosphorus atoms in a P−O−P linkage are called pyrophosphates. The general formula of pyrophosphate for SIBs is $Na_xM_y(P_2O_7)_z$ where M = transition metal (V, Mn, Fe, Co, Ni, or Mo); *x*, *y*, and *z* are integers, and $x > 1$.[84] Depending upon the transition metal choice and synthesis process pyrophosphates can crystallize in numerous structures like tetragonal, triclinic, and orthorhombic. Among them pyrophosphates of Fe, V, and Mn exhibit good electrochemical activity relative to phosphates because of the greater stability of the $P_2O_7^{4-}$ group, but their rate capabilities, crystallinity, and theoretical specific capacities are comparatively poor. Pyrophosphates are energetically more stable than orthophosphates at high temperatures as orthophosphates get decomposed between 500 and 550 °C to form pyrophosphates when exposed to air.[85] Pyrophosphates are better than oxides as their unit cell parameters are always greater, which means they have a large spatial structure which allows free mobility of ions. They have an open framework structure which facilitates facile ion transport pathways and are an attractive energy storage material. The most common type of defect which is found in this pyrophosphate framework is an antisite defect where the alkali cations and M ions exchange positions, and for this very low activation energy is required suggesting long-range and 3D (Na ion) diffusion.[86] Okada et al.[87] reported $NaVP_2O_7$ having specific capacity of only 38.4 mA h g^{-1} at C/20 with the average V^{4+}/V^{3+} redox potential centered at 3.4 V in which octahedral (VO_6) units are linked with five P_2O_7 groups, which is less than the theoretical specific capacity 108 mA h g^{-1}. The reason behind such an observation is the lowering of the miscibility gap between the sodiated and desodiated phases and inherent high resistance.

https://doi.org/10.1021/acsomega.4c02709
ACS Omega 2024, 9, 22509−22531

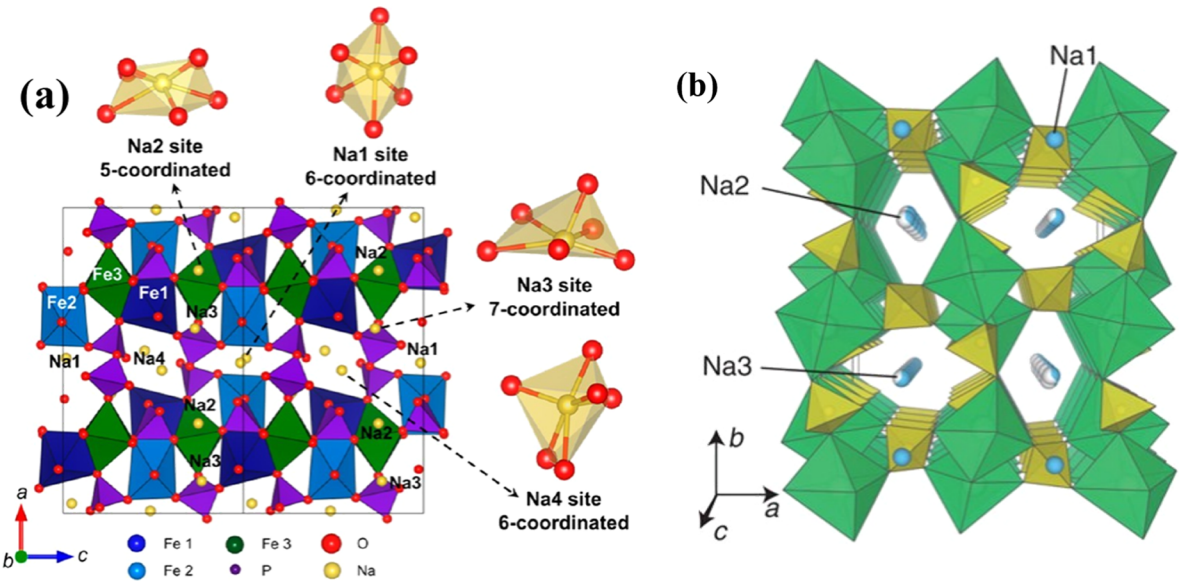

Figure 7. (a) Schematic representations of $Na_4Fe_3(PO_4)_2(P_2O_7)$. Reprinted with permission from ref 90, copyright 2013, American Chemical Society.[90] (b) Structural framework of $Na_2Fe_2(SO_4)_3$. Reprinted with permission from ref 96, copyright 2014, Nature Communications.[96]

$Na_{3.64}Fe_{2.18}(P_2O_7)_2$ was reported by Bolei et al.[88] to have a remarkable reversible capacity of 99 mA h g^{-1} at 0.2C, an exceptional cycling life retention of 96%, and a high Coulomb efficiency of over 100% even after 1000 cycles at 10C. Here, a 3D network structure comprised of FeO_6 and PO_4 links together to form a huge tunnel that facilitates Na^+ ion movement.

2.4. Orthophosphate. The compounds which contain only one phosphorus unit or the simplest form of phosphorus are called orthophosphate. The general formula of orthophosphate for SIBs is $NaMPO_4$, where M = Transition metal. Among all possible transition metals Fe was the first one to be studied, i.e., $NaFePO_4$, and it was found to exist in two forms—olivine and maricite. These forms were composed of PO_4 tetrahedra and FeO_6 octahedra crystallized in the orthorhombic space group *Pnma* with distinct unit cell parameters. Although the maricite phase is thermodynamically stable as compared to olivine it is electrochemically inactive as it lacks Na^+ ion diffusion channels due to the structural arrangement. In the maricite phase the adjacent octahedral units are shared on the edges, which are further connected with tetrahedral units to share the corners, whereas in the olivine phase the corner-shared octahedral units are connected with tetrahedral units.[84,85] The olivine phase of $NaFePO_4$ shows 80% theoretical capacity that is of 125 mA h g^{-1}.[68]

2.5. Mixed Phosphates. These are the compounds with the general formula $Na_4M_3(PO_4)_2P_2O_7$ (M: transition metals) having a three-dimensional orthorhombic structure made up of PO_4 tetrahedra and MO_6 octahedra that share corners with the pyrophosphate group through a P−O−P interlayer link are called Mixed phosphates. Recently, Mixed phosphates have caught scientists' attention as a new class of SIB cathode materials because of their long lifetime, small volumetric strain, and higher operating voltage than existing polyanionic materials. When compared to a 1D channel possible in other polyanions, the 3D channels in a mixed polyanion have four Na^+ sites which allows fast Na^+ diffusion.[89] The schematic illustration of Figure 6. Potentially, a unique cathode may result from the tunability of structure through the inclusion of different combinations of polyanions. However, during the electrochemical reaction, the redox reaction in materials frequently involves complicated structural evolutions that needs to be studied further.[90] In this case due to the mixing of some other element the redox potential of M metal is increased independent of cationic size and redox activity of 3d metal substituents, which was earlier possible only by the addition of a more electronegative element.[91] Hyungsub et al.[92] reported $Na_4Mn_3(PO_4)_2(P_2O_7)$ having the highest redox potential of 3.84 V among the reported Mn-based cathodes with an energy density of 416 W h kg^{-1}. The reason for this increment is the low-activation energy barrier during 3D Na diffusion during charging at several states of charge of the $Na_{4-x}Mn_3(PO_4)_2(P_2O_7)$ electrode (where x = 0, 1, 3). In contradiction to various Mn-based electrodes where Na ion migration is decreased due to the structural change by Jahn−Teller distortion (Mn^{3+}), here no decrement is observed; in fact, it helps by opening up Na diffusion channels.[92] The reversible capacity of $Na_4Fe_3(PO_4)_2P_2O_7$/C (NFPP) (a schematic representation of this material is given in Figure 7(a)) cathode material was initially reported by Kim et al.[93] in SIBs, where it showed a capacity of 113.5 mA h g^{-1} at 0.1C. The correlation between the Na ion extraction and structure is shown in Table 2.

Table 2. Order of Sodium Extraction from the Structure of $Na_xFe_3(PO_4)_2(P_2O_7)$ ($1 \le x \le 4$)

composition	space group	Na1 site	Na2 site	Na3 site	Na4 site
$Na_4Fe_3(PO_4)_2(P_2O_7)$	$Pn2_1a$	1.0	1.0	1.0	1.0
$Na_3Fe_3(PO_4)_2(P_2O_7)$	$Pn2_1a$	1.0	0	1.0	1.0
$Na_2Fe_3(PO_4)_2(P_2O_7)$	$Pn2_1a$	0.5	0	1.0	0.5
$NaFe_3(PO_4)_2(P_2O_7)$	$Pn2_1a$	0	0	0.5	0.5

Wen et al.[94] developed NFPP having a reversible capacity of 118 mA h g^{-1} at 0.2C, and even at the high scan rate of 20C it shows 64 mA h g^{-1} capacity and a capacity retention of 79.6% over 10,000 cycles at 10C. With a hard carbon anode and NFPP cathode, the full cell shows a reversible capacity of 126.4 mA h g^{-1} at 20 mA g^{-1} and a high operating voltage of 2.9 V.[95]

2.6. Sulfates. Polyanionic materials $(Na_xM_y(XO_4)_n$; M is transition metal; X = Si, S, P, W, As, Mo) consist of a series of

https://doi.org/10.1021/acsomega.4c02709
ACS Omega 2024, 9, 22509−22531

tetrahedral units of anion $(XO_4)^{n-}$ and other derivatives. These materials are categorized into sulfates, silicates, mixed phosphates, phosphates, pyrophosphates, etc. Polyanionic sulfate cathodes, because of the high electronegativity of sulfur, exhibit relatively higher $M^{n+}/M^{(n-1)+}$ redox potentials in comparison with the majority of different stated cathodes.[97] Sulfate-based polyanions are not prepared using conventional methods of high-temperature solid state in aqueous media due to reasons such as low thermal stability at high temperatures (i.e., above 350 °C) and hygroscopic properties of sulfates. This has resulted in inexpensive, sustainable synthesis using techniques like ball milling, solvothermal method, and a low-temperature solid-state pathway, which decreases the cost and energy consumption and contributes in its commercialization.[97,98]

2.6.1. Fe-Based Polyanionic Sulfates. Among the most distinctive members of the category are Fe-based polyanionic sulfates consisting of several crystal structures such as crystal water-containing bloedite- and krohnkite-type sulfates and a crystal water-free alluaudite/eldfellite phase.[97] Along with the high inductive effect provided by the S, high energy density can be obtained by enhancing the number of sulfate groups.[99] Thus, various bi-, tri-, and polysulfates were synthesized in different studies.

The excellent redox potential of Fe^{2+}/Fe^{3+} (3.6−3.9 V vs Li/Li^+) in Li-based polyanion sulfate cathodes became the inspiration to explore Na-based bisulfates.[100] However, due to high moisture sensitivity, bisulfates are likely to form hydrated derivatives when they come in contact with air. $Na_2Fe(SO_4)_2\cdot nH_2O$ is synthesized by the dissolution of Na_2SO_4 and $FeSO_4\cdot 7H_2O$ in DI water, then heating the mixture at 70−90° to give a saturated solution. The hydration degree n = 4 ($Fe(SO_4)\cdot 4H_2O$) can be obtained by precipitating the final product by adding alcohol, while hydration n = 2 can be obtained without using the hydrophobic alcohol media.[99,100] The $Na_2Fe(SO_4)_2\cdot 4H_2O$ stabilizes in a monoclinic structure with a bloedite atomic arrangement. The $P2_1/c$ monoclinic framework is composed of four O atoms linking to two H atoms together with isolated $MO_2(OH)_4$ octahedral units within the octahedra and the rest two O atoms connected to SO_4 tetrahedra. Large vacancies are filled by the Na^+ ions. The $Na_2Fe(SO_4)_2\cdot 2H_2O$ assumes a $P2_1/c$ krohnkite framework, along with isolated $MO_2(OH)_4$ octahedra with four O atoms that are attached to four sulfate tetrahedra and two O linked with two H. This arrangement creates pathways for Na ion migration.[100] Careful dehydration of $Na_2Fe(SO_4)_2\cdot 4H_2O$ leads to formation of $Na_2Fe(SO_4)_2$ also forming a lattice with Na ion in large cavities.

A new class of polyanionic sulfate cathode, $Na_2Fe_2(SO_4)_3$, reported by Barpanda et al. in 2014 having high redox potential of almost 3.8 V (vs Na), over 100 mA h g^{-1} reversible capacity, and an alluaudite-type structure is given in Figure 7(b).[96] Solid-state synthesis is one method of producing a polyanion that involves the annealing of 2/3 molar mixture of Na sulfate and Fe sulfate.[99] The polyanion assumes an alluaudite type structure (monoclinic; $C2/c$) having general equation $Na_{2+2x}Fe_{2-x}(SO_4)_3$. The alluaudite-type arrangement has edge-sharing FeO_6 octahedral units that are bridged together by SO_4. This creates a 3-D framework with large channels running in line with the c axis.[101] The $Na_{2+2x}Fe_{2-x}(SO_4)_3$ polyanion cathodes have exceptional rate kinetics due to the existence of quick migration routes for Na ion. One explanation for the high redox potential is the unique 3-D framework having a short Fe−Fe bond length and the presence of multiple electronegative sulfate units.[102]

Fe-based sulfates are electromagnetically active cathodes with high redox potential, relative elevated capacity, safe, inexpensive, and have sustainable methods of synthesis.[97,99] Nevertheless, they are sensitive to moisture, have poor conductivity, and decompose easily at high temperatures limiting their storage and synthesis.[97] Numerous studies contributing to develop improved polyanions have been done, for example, a $Na_{2.26}Fe_{21.87}(SO_4)_3$ phase was developed in which the Na^+ storage was improved by tuning the exposed crystal plane, resulting in a cell voltage of 2.35 V, an initial discharge capacity of 83.9 mA h g^{-1}, and capacity of 24 mA h g^{-1} (after 40 cycles).[103] A firm graphene $Na_{2+2x}Fe_{2-x}(SO_4)_3$ was assembled through a spray-drying method at low temperature resulting in enhanced stability and high conductivity as well as reversible capacity and better rate performance.[104] Fe-based polyanionic sulfate cathodes offer a strong foundation for material discovery and are among the cathode materials with the most potential for SIB development in the future.

2.6.2. Mn-Based Polyanionic Sulfates. Mn-based sulfates have attracted researchers because of their inexpensive cost, high natural abundance, reversible electrochemical activity, high intercalation voltage, and theoretical capacity. They are considered as one of the most promising options available for high-voltage cathodes.[97,101] The synthesis of Mn-based polyanionic sulfates is difficult due to the large size of Mn^{3+} ions as compared to Fe^{2+} and high degree of Jahn−Teller distortion resulting in large lattice deformation.[97,98] The two systems, $Na_2FeMn(SO_4)_3$ and $Na_{2.5}(Fe_{1-y}Mn_y)_{1.75}(SO_4)_3$, have been evaluated for their electrochemical performance and have an alluaudite-type structure in which Na^+ ions are present in three crystallographic positions. $Na_2FeMn(SO_4)_3$ delivers a capacity of about 110 mA h g^{-1} with an average voltage of 3.6 V. In a sequence of nonstochiometric $Na_{2.5}(Fe_{1-y}Mn_y)_{1.75}(SO_4)_3$ solid mixtures, there is gradual increase in average operation voltage with increasing Mn substitution, but the capacity drops dramatically. This is due to the inactivity of Mn^{2+} during cycling, and the charge compensation relies solely on the $Fe^{3+/2+}$ redox pair.[105]

Mn-based sulfates face drawbacks such as low electronic conductivity and low performance in SIBs, irrespective of whether they exhibit reversibility or cycling stability. This issue can be approached with solutions such as carbon coating and doping, which are going to need considerable research in the future. Usually, sulfates are synthesized below 450 °C often resulting in the presence of impurity and off-stoichiometric phases. In order to improve their crystallinity, thermal stability, and purity, excess Na or carbon sources can be added during synthesis.[105] Low price, high annual production, and high capacity make Mn-based polyanions one of the standout candidates for polyanionic sulfate cathodes.

2.6.3. Cu-Based Polyanionic Sulfates. Cu-based polyanionic sulfates are another candidate along with Fe- and Mn-based sulfates which may be utilized in extensive energy storage devices. To delve deeper into the inactivity of Cu-based polyanionic sulfates in Na^+ storage and migration, Kovrugin et al.[105] conducted theoretical calculations to explore the potential kinetic mechanism of $Na_2Cu(SO_4)_2$. It was found that the theoretical capacity was around 89 mA h g^{-1}, and the redox potential is 4.7 V (versus Na), which is outside the stability window of the electrolytes makes it an unacceptable cathode.[106] In another study, $Na_2Cu(SO_4)_2$ and its water derivative $Na_2Cu(SO_4)_2\cdot 2H_2O$ were prepared, and their redox mechanism was observed. The high Jahn−Teller distortion of Cu^{2+} along

https://doi.org/10.1021/acsomega.4c02709
ACS Omega 2024, 9, 22509−22531

with high redox potential lead to minimal (de)intercalation capacity.[107] The possible solutions to address the issue related to Cu-based polyanions include alteration of carbon content in electrode or structuring cathode compound at nanoscale.[107] Cu-based polyanionic cathodes are relatively inexpensive and may emerge as potential battery electrodes that involve conversion redox reactions

2.7. Fluorine Transition-Metal Salt. Increasing the energy density is an important factor to improve the energy density of the polyanionic material. Incorporating strongly electronegative anions to the polyanionic compounds is one of the ways to boost the redox potential of the material. Due to its strong ionicity, F^- can be considered because it not only results in a significant energy difference between the antibonding orbitals and the vacuum but also weakens the bond between M and O, raising the redox potential.

2.7.1. Fluorophosphates. A new class of fluorophosphates ($Na_3V_2(PO_4)_2F_3$, $NaVPO_4F$, and $Na_3(VO_{1-x}PO_4)_2F_{1+2x}$ ($0 \le x \le 1$)) with 3D sodium intercalation and improved electrochemical characteristics, such as high theoretical capacity and energy density, is produced when electronegative fluorine atoms are added to sodium vanadium phosphate.[70]

2.7.1.1. $NaVPO_4F$. There are two polymorphic phases of sodium vanadium fluorophosphates (NVPFs): the tetragonal phase at elevated temperature and the monoclinic phase at low temperature. Barker et al. reported the tetragonal NVPF with space group I_4/mmm, discharge voltage of 3.7 V, and initial capacity of 82 mA h g^{-1}.[80] Later, Zhero et al. created $NaVPO_4F$ in a monoclinic phase with $C2/c$ as space group and a specific capacity of 83.3 mA h g^{-1}.[81,82]

The XRD of $NaVPO_4F$ matched with NASICON (Na supersonic conductor) structured $Na_3V_2(PO_4)_3$. They both displayed comparable electrochemical performance at various plateaus of voltage.[83] Numerous carbon coatings and ion substitutions of metals were conducted to enhance the electrochemical performance of NVPF. According to Lu et al., NVPF/C has a higher capacity of 97.8 mA h g^{-1} for NVPF/C than pristine NVPF. In a similar manner, Ruan et al. improved electrochemical performance by graphene sheet coating. Zhero et al. also denoted improvement in monoclinic NVPF after doping Cr^{3+} into V positions. Additionally, Al doping also improved the performance compared to Al-free NVPF.[84] Jin and his colleagues used electrospinning to create $NaVPO_4F$/C nanofibers that had a high capacity (about 126 mA h g^{-1} C), good rate efficiency (about 61 mA h g^{-1} at 50C), and a long-life cycle. Outstanding electrochemical performance of $NaVPO_4F$/C resulted from the presence of small nanoparticles (about 6 nm) embedded within the pore-filled carbon. These nanoparticles effectively enhanced the kinetics of Na ion diffusion.[85]

2.7.1.2. $Na_3(VO_{1-x}PO_4)_2F_{1+2x}$ ($0 \le x \le 1$). $Na_3(VO_{1-x}PO_4)_2F_{1+2x}$ ($0 \le x \le 1$) is a novel family of vanadium oxy fluorophosphates, created by substituting oxygen in Na_3VPF. This new family contains the V^{3+} and V^{5+} extremes and the intermediate valence phases V^{3+}/V^{4+}. $Na_3(VO)_2(PO_4)_2F$(N_3VOPF) is preferred due to the high energy density and stability in cycling. Sauvage et al.[108] and Massa et al.[109] were the first to independently report it while assuming a tetragonal frame with symmetry I_4/mnm. After that Tristin et al. found the occurrence of N_3VOPF polymorph with the $P4_2/mnm$ space group. Its electrochemical performance was initially reported by Sauvage et al. in 2006 displaying two step plateaus of voltage between 3.6 and 4.0 V relative to Na/Na^+.[86]

In 2012, Rojo and group introduced the family of $Na_3(VO_{1-x}PO_4)_2F_{1+2x}$ materials as cathode for sodium ion batteries.[87] After that the existence of Na_3VOPF with mixed-valence V^{3+}/V^{4+} was introduced by Qi et al.[110] and Park et al. Single-crystalline 3D nanostructured $Na_3(VO)_2(PO_4)_2F$ was formed using VO_2 arrays, which demonstrated superior rate capability of 45 mA h g^{-1}, rapid ion transport, and a little volume change during the process of charging and discharging.[88] Park et al. discovered that the behavior of samples varied with the presence of F after studying numerous redox transitions between V^{4+}/V^{3+} and V^{5+}/V^{4+} redox reactions and Na.[89] It has been found that when oxygen was swapped out for Cl in $Na_3V_2Cl_2(PO_4)_2F$, the energy density rose from 520 to 758 W h kg^{-1}. Na_3VOF cathode suffered from poor intrinsic electronic conductivity which was improved by surface coatings, additives, and nano structuring.[90,91] Nanowires of RuO_2 coated with Na_3VOPF which enhanced capacity (120 mA h g^{-1}), cyclic stability, and rate capability (95 mA h g^{-1} at 20 °C rate) were reported by Peng et al. On doping Ru in Na_3VOPF hollow microspheres improved the electrochemical performance.[92] In 2020, Liang et al. were the first to report the discovery of an electroactive fluorophosphate, $Na_5V(PO_4)_2F_2$. Through ex-situ XRD and DFT analysis, they investigated the sodium extraction mechanism and discovered that the charging process involved a two-phase reaction followed by a single-phase reaction.[93] Mazumdar et al. conducted a theoretical study employing DFT calculations to investigate the process in which sodium is extracted from the phases $Na_5M(PO4)_2F_2$ (Value of M is Cr and V). Their findings revealed that the extraction of greater sodium content necessitates elevated voltages of 4.77 V for the Cr-based phase and 4.56 V_{Na} for the V-based phase.[94] Fang et al. investigated the effects of particle shape on the intercalation characteristics of $Na_3V_2(PO_4)_2F_{3-y}O_y$. They employed scanning electron microscopy (SEM) to observe various morphologies including nanospheres (NVPF1), cylindrical agglomerates (NVPF2), micrometric flakes (NVPF3), and sand roses (NVPF4). Sand roses and nanospheres demonstrated improved electrochemical performance, especially in terms of high-rate performance. Accessibility to Na^+ diffusion tunnels was cited as the cause of this better performance.[95]

2.7.1.3. Other 3d Metal-Based Fluorophosphates. Comparing V-based cathodes, the redox potential of different 3d metals were compared (M = Fe, Co, Mn, Ni), and it was observed that they have lower redox potential. The PO_4^{3-} was replaced with PO_4F^{4-} to provide a different structural framework. The Nazar group first reported the crystallization of Na_2FePO_4F, which belongs to the *Pbcn* orthorhombic space group. They found that Na^+ ion migrates very quickly in the *ac* plane, with only 3.7% volume variation during deintercalation. Further studies were done by Tereshchenko et al. using XRD and DFT calculations which showed that Na_2FePO_4F adopted intermediate monoclinic $Na_{1.5}FePO_4F$. DFT calculations confirm that Na_2FePO_4F crystallizes in space group *Pbcn* and $Na_{1.5}FePO_4F$ crystallizes in P_{21}/c space group. The structure of Na_2FePO_4F was found to have two distinct Na sites: the electrochemically active Na_2 site and the inert Na_1.[96] Na_2CoPO_4F was first prepared in 2010, but its electrochemical reversibility is poor. Later Komeba et al. synthesized differently modified Na_2CoPO_4F, but it exhibited irreversible capacity and lower cyclic stability.[97] Since then, Lang's team has used a space-drying method to prepare pure-phase Na_2CoPO_4F/C composites, but they had the ability to degrade quickly. Although it is considered a promising high-

https://doi.org/10.1021/acsomega.4c02709
ACS Omega 2024, 9, 22509−22531

voltage cathode, there are still many challenges in improving its stability and reversibility.[97]

In the 3D tunnel structure, Na_2MnPO_4F was discovered to crystallize with the $P21/n$ space group; this was first reported by Recham et al. and Ellis et al. Upon further investigation by Kim et al. about its functionality, it was discovered that there are three Na-ion diffusion pathways and four distinct interstitial Na sites: the Na1−Na4 chain, the Na2−Na3 chain, and the interchain, each with activation barrier of 600, 500, and 400 meV, respectively.[73] Research has indicated that the considerable polarization and low electrochemical activity of Na_2MnPO_4F make it unsuitable for widespread use. Consequently, more investigation is required to enhance its electrochemical performance.

2.8. Fluorosulfates. Sulfate chemistry has become increasingly popular in the advancement of high-voltage electrode materials for SIBs. In 2010, Tarascon and group proposed a novel class of polyanionic materials called fluorosulfate, with the formula A_xMSO_4F (A = Li/Na; M = 3d metal). Their research was driven by the inductive effect, which is achieved by polyanions with more electronegativity.[70] Fluorosulfate can be synthesized through various methods, including solid-state reaction, ionothermal synthesis, polyol-assisted synthesis, and dehydration of $NaFeSO_4F{\cdot}2H_2O$. $NaFeSO_4F$ exhibits a tavorite-like structure (maxwellite-like structure) with monoclinic structure ($C2/c$). Its crystal lattice is constructed from corner-sharing FeO_4F_2 octahedra connected to SO_4 tetrahedra, forming tunnels capable of storing Na ions.[111]

Tasrascon and group demonstrated the electrochemical activity of $NaFeSO_4F$ in sodium ion batteries relying on the $Fe^{II/III}$ redox couple at 3.5 V_{Na}. Kim and colleagues discovered a novel polymorph of $NaFeSO_4F$ with a triplite-type crystal structure, featuring an elevated operational voltage of 3.7 V_{Na} and superior electrochemical performance when compared to the tavorite polymorph. The triplite $NaFeSO_4F$ achieved nearly theoretical capacity around 138 mA h g^{-1} at a 0.01C rate. This improved performance was attributed to variances in the positioning of fluorine within the FeO_4F_2 octahedra.[112] Fluorosulfates represent a compelling avenue in the realm of cathode materials, drawing the attention of numerous research teams due to their remarkable high operating voltages. Nevertheless, the available structural data on fluorosulfates remains rather restricted, rendering it an ideal realm for the exploration of innovative, cost-effective materials like manganese (Mn)- and nickel (Ni)-based systems through diverse synthesis methods like hydrothermal and sol−gel processes.

2.9. Silicates. The basic structural unit of all silicates is a silicon tetrahedron in which each silicon is covalently bonded by four oxygen atoms having strong Si−O bonds. The general formula of silicates used in NIBs is Na_2MSiO_4 where M = Fe, Mn, Co. The silicate family consists mainly of parasilicates, metasilicates, and orthosilicates. Among all possible transition metals, Mn was the first to be explored in SIBs as Na_2MnSiO_4, which exhibits a capacity of 125 mA h g^{-1} due to the exchange of $1e^-$ at a rate of 0.1C (13.9 mA g^{-1}) within 2.0 to 4.0 V at 363 K, possessing a sufficiently high rate capability.[113] Orthosilicates' practical application is hindered due to its electrochemistry and complex crystal structure. Researchers have tried in several ways to improve its performance. Basit et al. utilized the cubic polymorphs of Na_2FeSiO_4 with $F\bar{4}3m$ symmetry supported on carbon nanotubes which in the voltage range of 1.5 to 4.5 V shows a capacity of 172.9 mA h g^{-1} at 0.1C and shows a remarkable capacity of 109.3 mA h g^{-1} at 20C.[114] The cause for these enhanced electrochemical capabilities is the structural stability of the complex, reduced particle size and charge transfer resistances, enhanced defect structure, high sodium-ion diffusion coefficient, and enhanced electronic conductivity thanks to carbon nanotubes. Sodium-based silicates are less explored as compared to Lithium-based silicates. Lithium-based silicates are explored with expected capacity because of a $2e^-$ exchange process,[115] whereas Sodium-based silicates lag behind because of the impure phases obtained during solid-state synthesis and low electronic conductivity.[113,116] To improve the performance in Sodium-based silicates, a solution-assisted synthesis method like refluxing and sol−gel assisted solvothermal techniques have been employed to synthesize silicate-family nanoparticles.

3. STRATEGIES TO IMPROVE THE ELECTROCHEMICAL PERFORMANCE

Even though polyanionic materials are considered as promising candidates in SIB cathode materials, they suffer from poor electronic conductivity as the metal octahedra is separated by phosphate tetrahedra. The electron transfer pattern follows a slower M−O−P-O-M pattern rather than a simple M-O-M pattern, and also the deposition of the discharged products affects the electrochemical performance specifically, lowering the rate capability of the materials. Also, the electronegativity of the anions affects the poor electronic conductivity in the framework. As the separation between the valence band and conduction band is large (1.735 eV) in $Na_3V_2(PO_4)_3$ assumed due the higher electronic affinity of the vanadium, it is found to have low electronic conductivity.[117] The limited capacity and the lower energy density due to the heavy inactive anionic group is another challenge faced by polyanionic materials. Introducing lighter molecular weight anionic groups or anions which can raise the redox potential values by a strong inductive effect can improve the energy density. The introduction of ions which can activate multielectron redox reaction also results in improved energy density.

3.1. Nanostructuring. One of the reasons for capacity loss in the cathode materials is the presence of dead corners. The larger the size of the electrode particles, the more dead corners that are not going to participate in reaction, and more will be the diffusion distance for Na^+ ions. Shortening sodium ion diffusion pathways by controlling the dimension of the active material is one the successful and common strategies to enhance the electrochemical performance.[118] This increases the surface area and thus reactive sites of the active material and reduces the ion diffusion pathways. Kim et al. reported that previously regarded inactive maricite $NaFePO_4$ shows electrochemical properties (capacity 142 mA h g^{-1}) when downsized to nanoscale. After the first extraction of Na ions, the maricite $FePO_4$ converts into amorphous $FePO_4$ which provides a smaller barrier for Na ions to hop from one site to another.[73] Law et al. reported improved electrochemical performance of nanostructured Na_2FePO_4F in comparison to the a pristine sample. The soft template method was used to prepare nanostructured Na_2FePO_4F, which was then heat-treated and subjected to high-energy ball milling. The BET analysis showed doubled surface area of 40.0 m^2 g^{-1} in comparison to the pristine sample (22.2 m^2 g^{-1}). Also, the relatively low percent of antisite disorder leads to improved Na diffusion due to availability of diffusion channels in different orientations. The nanostructured sample showed a capacity of 116 mA h g^{-1} at 0.1C and a capacity retention of 80% after 200 cycles at 1C. The improvement at nanoscale can be attributed to

https://doi.org/10.1021/acsomega.4c02709
ACS Omega 2024, 9, 22509−22531

its high surface area, small size, low concentration of antisite disorder, and improved transport properties.[119] NASICON-type $Na_3V_2(PO_4)_3$ is usually synthesized by high-temperature calcination, which results in the formation of particles greater than 2 μm; this leads to poor conductivity in turn resulting in lowering the rate capability.[120] Decreasing the particle size to nanoscale can reduce the Na^+ diffusion distance and thus improve the transport kinetics. Choosing a lower calcination temperature can result in smaller particle size, but it results in lowering the crystallinity of particles.[121] When compared to the microstructured particles, nanosized particles lack tap density and energy density due to more surface side reaction.[122,123] Micro nano hierarchical structures having sufficient pores and ion diffusion channels are the best option to alleviate this.[124] An NVP of such type was prepared by Kuppan et al.[121] using an aqueous precipitation method with low annelation temperature and crystallization time. The prepared NVP/C material demonstrated improved cyclic and storage performance with capacity of 62 mA h g^{-1} at 40C and 50% capacity retention after 30,000 cycles. The facilitated sodium ion transport in the nanosized carbon-coated porous NVP particles is responsible for the material's exceptional electrochemical characteristics. Reducing the size of the particles can improve the kinetics of the electrochemical processes as well as the usage of active materials. The relation between diffusion time and diffusion length is given as

$$\tau = \frac{L^2}{D_{Li}}$$

Decreasing the diffusion length will decrease the diffusion time for a D_{Li} leading to long-term cyclability and high-rate capability.[125] Nano NVP@C prepared by Wenchao et al.[126] gave a lower value of the potential polarization (ΔE = 31 mV), which is also comparable to the value of $LiFePO_4$, as compared to other NVPs. Such a low value is attributed to lower polarization and easier migration of Na ions due to its nano size and carbon coating. The prepared NVP@C gave a capacity retention of 99.6% at 0.5C after 50 cycles. It also displayed long-term cyclic stability with initial discharge capacity of 94.9 mA h g^{-1} and a capacity retention of 96.1% after 700 cycles at 5C. This can be explained by its distinct porous nano core−shell structure. Therefore, the findings so far suggest that tiny nanoparticles can achieve high active material utilization and reduced diffusion pathways and, ultimately, lead to improved electrochemical performance.

3.2. Surface Coating. Nanosizing of the active material leads to unwanted side reaction with the electrolyte, as the increased surface area of the active material results in heightened interactions. Surface coating is a common strategy to enhance electronic conductivity as well as to protect the active surface from the electrolyte attack. Surface coating helps in the following ways. 1. Coating with a material having high electronic conductivity improves the electron transfer at the surface of the active material but blocks the electron transfer between the active material and the electrolyte (so the compounds where the E_g is less than 0.5 eV is not preferred).[127] 2. Dissolution of the active material with the electrolyte can be reduced. 3. Reduces the unwanted side reaction of active material with the electrolyte; thus, deposition of the impurities on the electrode surface can be minimized. 4.Coating provides mechanical strength to the active material, act as a binder, and prevents the fragmentation of the active material. 5. Prevents the agglomeration of the particles during charge−discharge, thus improving the rate capability and cyclic stability of the material.[128] A coating layer should possess chemical properties to prevent the side reaction between the coating layer and active material or electrolyte along with high reduction potential.[129]

Coating the surface of active material with thin-layer carbon, metal oxide, and conducting polymer has been found to significantly enhance the electrical conductivity of the material to a larger extent. The physical properties of the coating as well as the homogeneity and the thickness of the coating highly affect the electrochemical properties of the coated cathode materials.[129] Due to higher electronic conductivity carbon coating in the polyanionic compounds is found to enhance the rate capability and the cyclic stability of the material. The interconnected open pores of the carbon frameworks favor the electrolyte absorption and also formation diffusion pathways for the charge carrier ions.[130] The robust and flexible carbon framework reduces the volume changes associated with the intercalation and deintercalation of sodium during a charging−discharging cycle.[131] To attain a homogeneous carbon coating in a polyanionic compound, organic carbon sources such as citric acid,[132] ascorbic acid,[133] glucose,[134] and vitamin C[135] are being employed. The coating of hard carbon,[136] carbon nanotube (CNT),[137] graphene oxide,[133] and amorphous carbon[136] will form a conductive framework in the material which increases the electronic conductivity which in turn improves the electrochemical performance. Chen et al. synthesized CNT-decorated NVP particles covered by amorphous carbon layers by spray-drying and carbothermal reduction methods which enhanced electrochemical performance. This improvement can be attributed to the decreased charge transfer resistance and ohmic resistance due to CNT coating. In addition, the decreased particle size and the induced porous structure caused by the coating of CNT increases the area of contact between the electrolyte and the NVP particles, which in turn helps in the easy diffusion of electrons between the particles. Along with this, the higher amount of graphitized carbon in CNT also enhances the electronic conductivity in the material.[137] Tang et al. explored the CNT coating in pyrophosphate by the spray-drying method and analyzed the electrochemical performance in half cell and full cell. $Na_4Mn_2Co(PO_4)_2P_2O_7$ with different ratios of carbon nanotube (CNT) such as 3, 5, and 7 wt % were prepared. Among them, sample with 5% of CNT (NM2CPP/C−CNT) shows the best performance with a reversible initial discharge capacity of 96.1 mA h g^{-1} and an energy density of 371 W h kg^{-1} at 0.1C. NM2CPP/C microsphere structure nanoparticles were found to have an average size of 150 nm, and they are interconnected in the CNT network. The carbon coating helps in preventing the electrolyte corrosion of the material by separating bulk material from the electrolyte. The coexistence of the CNT and amorphous carbon facilitate the facile transport of sodium ions and electrons which leads to the enhancement of the electrochemical performance.[138] Fang et al. synthesized CNT-coated Na_2FeSiO_4 microspheres which show a specific capacity of 168.7 mA h g^{-1} at 0.1C and an excellent cyclic stability. The enhanced electrochemical performance is due to the formation of conductive transport pathways for electrons and Na^+ ions as a result of CNT coating.[139]

Graphene oxide is a viable option for carbon matrix for polyanionic compounds due to the larger surface area and numerous surface functionalities which allow the deposition of the electrode materials.[133] Rui et al. synthesized carbon-coated $Na_3V_2(PO_4)_3$ nanocrystals wrapped in reduced graphene oxide

https://doi.org/10.1021/acsomega.4c02709
ACS Omega 2024, 9, 22509−22531

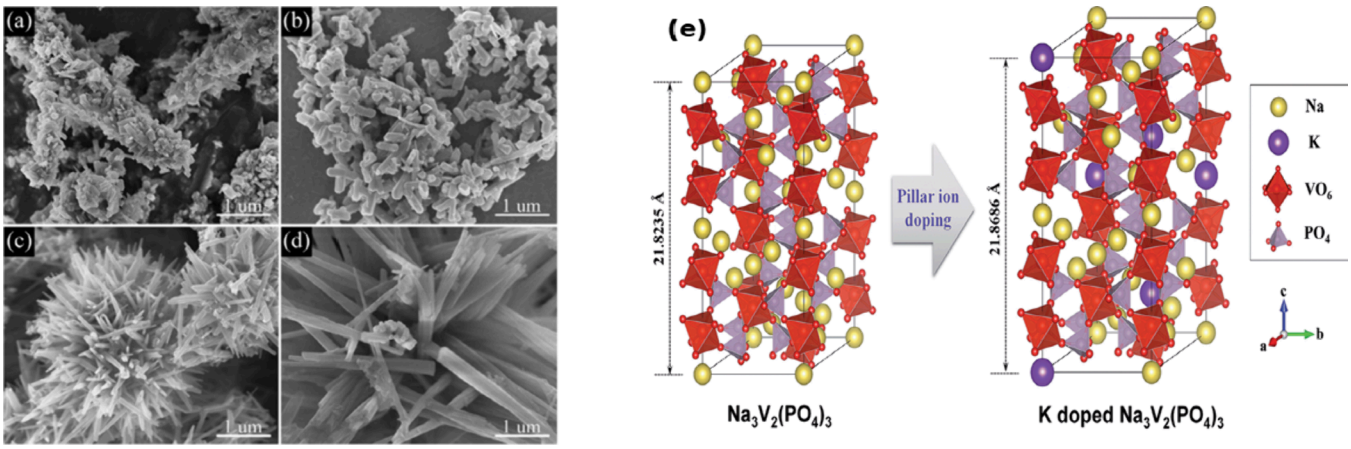

Figure 8. SEM images of the as-synthesized Na_2FePO_4F samples. SEM images of (a) $Na_2FePO_4F_{-8.5}$, (b) $Na_2FePO_4F_{-9.5}$, (c) $Na_2FePO_4F_{-10.5}$, and (d) $Na_2FePO_4F_{-11.5}$. Reprinted with permission from ref 141, copyright 2017, Elsevier.[141] (e) Schematic illustration of doping of K^+ into Na sites in $Na_3V_2(PO_4)_3$. Reprinted with permission from ref 143, copyright 2014, Royal Society of Chemistry.[143]

through a freeze-drying method. The synthesized material shows specific capacity of of 86 mA h g^{-1} at 100C and 64% capacity retention after 10,000 cycles at 100C with an electrical conductivity of ≈110 S m^{-1}. The enhanced electrochemical performance of the material is considered due to the highly conductive nature of the rGO and shortened diffusion pathways due to the reduced nanograin size, and the micro/mesopore structure provides the fast ion transport.[140]

Chen et al. synthesized in situ carbon-coated $Na_2FeP_2O_7$ coated with reduced graphene oxide through a freeze-drying method. The prepared compound exhibits a capacity of 65 mA h g^{-1} at 10C and almost full capacity retention at 1C.[133]

Chen et al. synthesized hard carbon wrapped $Na_3V_2(PO_4)_3$@C, which shows an excellent electrochemical performance with a discharge capacity of 111.6 mA h g^{-1} at 1C and a capacity retention of 83.3% over 3000 cycles at 40C. The NVP@C size decreased from 2 to 3 m to 500−800 nm subsequent to hard carbon coating, which clearly shows that the higher calcination temperature used for the formation of hard carbon has restricted the particle growth of NVP thus increasing the electronic and ionic conductivity. The increased reversible capacity of NVP@C@HC (111.6 mA h g^{-1}) over NVP@C (101.7 mA h g^{-1}) indicates that the double carbon coating increases the reversibility of Na^+ insertion/extraction. The electrochemical studies also show that a carbon layer accommodates a large volume change during charging and discharging.[139]

Rui Ling et al. synthesized Na_2FePO_4F/C by a solvothermal method which exhibits a discharge capacity of 114.3 mA h g^{-1} at 0.1C and cyclic stability of 93.3% after 100 cycles. Morphology changes of the material as the pH of the precursor solution changes and also due to the effect of carbon coating were investigated by the group. As the pH increased from 8.5 to 11.5 the morphology of the active material changed from rod-like to slender needle-like crystals. Change in the morphology along with pH is given in Figure 8(a−d). As a result of carbon coating, the surface area increased as the cylindrical particles fractured into spherical nanoparticles. The synthesized Na_2FePO_4F/C at a pH of 10.5 shows the highest surface area of 126.2 me^2 g^{-1} and reduced particle size to 10−100 nm owing to its better electrochemical performance. The enhanced electrochemical performance is a cumulative effect of carbon coating and reduced particle size where the carbon coating changes the crystallographic orientation resulting in the reduced migration resistance of sodium ions and charge transfer resistance.[141]

In short the improved electrochemical performance can be explained as a porous carbon matrix functioning as an elastic buffer, reducing the strain of volume changes during Na intercalation and deintercalation leading to a high cyclic performance. This also resulted in a 3D porous interconnected framework, facilitating electrical contact as well as Na-ion conduction.[23,142]

Heteroatom doping to the carbon framework further improves the ionic/electronic conductivity by increasing the interlayer spacing of the of the carbon thus providing enough space for intercalation-deintercalation of sodium ions. In addition, heteroatom-doped carbon materials possess numerous lattice defects, which improves the electrochemical reaction kinetics and, thus, the cyclic stability and efficiency of the material. Wei Li synthesized $Na_3V_2(PO_4)_3$ structure with sulfur-doped carbon layer (HP-NVP@SC) which shows a rate performance of 116.5 mA h g^{-1} at 1C and 91% capacity retention after 2500 cycles.[82]

Klee et al. have improved the stability of $Na_3V_2(PO_4)_3$ by coating 1.5% or 3.5% wt. of M_xO_y (Al_2O_3, MgO, and ZnO). Galvanostatic cycling half-cells show a significant capacity improvement for samples coated with 1.5% of metal oxides and good cycling stability as high as 95.9% for ZnO@$Na_3V_2(PO_4)_3$. The samples coated with 1.5% metal oxides show the least charge transfer resistance and surface area, according to the impedance spectra recorded following the first cycle; after 50 cycles, the surface layer and the charge transfer show a decrement in values compared to the first cycle. This is due to the formation of metal fluorides on the surface of the electrode, which protects the electrode degradation by HF and avoid a deleterious increase of the electrode resistance. The HF traces in the electrolyte lead to side reaction and electrode degradation. The scavenging effect of ZnO can be expressed as

$$ZnO + 2HF \rightarrow ZnF_2H_2O$$

The acidity of the electrolyte was reduced by the conversion of metal oxides into fluorides, hence delaying the cathode corrosion on cycling.[144]

3.3. Morphology Control. The morphology of the active material also plays an important role in affecting the rate performance of the material by improving the electronic

https://doi.org/10.1021/acsomega.4c02709
ACS Omega 2024, 9, 22509−22531

conductivity and structural stability. One-dimensional structures and architectures like nanofibers and nanowires have advantages like short diffusion distance of Na^+ ions. A large electrode−electrolyte contact area leads to easy access of the electrolyte and is able to accommodate the volume change thus increasing the cyclic stability.[145] Wenhao Ren et al. successfully achieved cyclic stability of 95.9% over 1000 cycles at 10C and a rate performance of 94 mA h g^{-1} at 100C from 3D $Na_3V_2(PO_4)_3$ nanofiber. The improved performance is explained due to both the electrochemical and mechanical advantages such as multichannel diffusion pathways for ions, enhanced structural stability, and uninterrupted electron transfer due to longitudinal paths for facile electron transfer.[146] Additionally, the 3D architecture represents a potent family to improve high rate capability. Typically, graphene materials are used to create 3D structures. Yu Meng et al. constructed the 3D graphene-based sandwich-like $Na_2Fe(SO_4)_2{\cdot}2H_2O$ composite which exhibits good rate performance and long cycle life. The improved electrochemical performance is attributed to easy transport of the electrons and reduced moisture sensitivity of the sulfates, which improves the structure stability which is related to the hierarchical sandwich-type nanoarchitecture.[147]

The particles of $Na_2Ti_3O_7$ possess a flower-like structure in three dimensions (3D), along with large specific surface area. They exhibit an open structure and nanoarchitecture, which contributes to their 3D morphology, in turn facilitating the diffusion of Na^+ ions and the wettability of electrolyte, resulting in exceptional rate performance. The microflower structure augments the specific surface area and the contact area with the electrolyte. This innovative 3D architecture effectively enhances the electron/ion transport kinetics of Na_2Ti_3O7 thereby ensuring the integrity of the electrode structure. The resultant outcome is outstanding electrochemical performance, characterized by long cycle life and high rate capability.[148]

Qiao et al. devised a porous structure for single-crystalline $Na_3V_2(PO_4)_3$ using the polymer-stabilized droplet method. This porous single-crystal structure significantly reduces the Na^+ diffusion distance and promotes ion transition, resulting in outstanding electrochemical properties (100 mA h g^{-1} at 0.5C, and 81 mA h g^{-1} at 1C after 10,000 cycles).[149] $Na_3V_2(PO_4)_3$ possesses a porous sponge-like structure with the highest surface area, which exhibits remarkable rate capability and high cyclic stability. Typically, a large surface area of an electrode leads to the formation of solid electrolyte interface (SEI), which can impede ion diffusion during battery operation. However, in this case, the primary factor influencing the electrochemical performance is the well-defined porous structure rather than the SEI layers. This phenomenon resembles the synergistic or antagonistic effect of a dopant on the electrochemical performances of multielectron materials.[150]

$Na_3V_2(PO_4)_3$/C hierarchical microspheres demonstrate excellent performance in terms of high-rate capability and cyclic stability in SIBs. This hierarchical architecture characterized by large surface area and numerous mesopores enables a significant electrode−electrolyte interaction and a short pathway for ion diffusion. The combined effect of large surface area, attractive structure integrity, and presence of a large interstitial space leads to the superior performance observed.[122]

Qiuyue Wang et al. constructed a honeycomb-type hierarchical porous microball (Figure 8) for $Na_3V_2(PO_4)_3$ by a one-pot synthesis, in which micro/mesopore interconnective nanochannels for fast transport of ions and increased electrolyte penetration were present in the spherical particle, which improves the electrochemical kinetics.[151] The morphology of the particles is found to be spherical, like microballs with a diameter around 3 μm according to SEM analysis, given in the Figure 9(a). The cross-sectional image of the microballs is

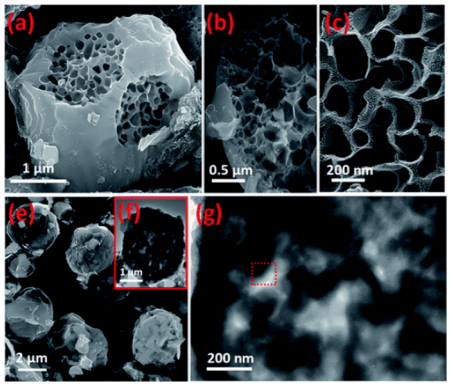

Figure 9. Morphologies of the honeycomb-structured $Na_3V_2(PO_4)_3$/C microball. (a) SEM image of the microball filled with hierarchical pores, (b) SEM image of its cross-section and (c) enlarged image of hierarchical pores, (e) low-resolution SEM image of the $Na_3V_2(PO_4)_3$ microballs and (g) its partial enlarged image. Reprinted with permission from ref 151, copyright 2015, Royal Society of Chemistry.[151]

shown in Figure 9(b), which depicts the presence of macropores inside the individual microballs with a size ranging from 100 to 200 nm. The walls of the macropores contain mesopores with a size ranging from 5 to 30 nm, which is responsible for the interconnection between the macropores as shown in Figure 9(c). Figure 9(e) is the low-resolution SEM image which confirms the uniformity of the material.[151]

The synthesis routes for nanosized phosphates are widely studied. One method is the hydrothermal method, which produces nanosized $NaFePO_4$ with a larger specific capacity. Another method is the sol−gel and coprecipitation method, which allows the control of special structures. These methods have been used to create materials with prolonged cycle life and superb energy density.[152] The conductive interconnected network and full contact between cathode and electrolyte is beneficial for boosting sodium-storage performance. Spray drying is utilized for preparing cathode materials with different morphologies and achieving hybridization with conductive materials. Other synthesis routes like the template method and electrospinning can prepare cathodes with special morphologies and remarkable performance.[153]

The commonly used high-temperature solid-state method generally gives particles having irregular shapes and larger ones. It is challenging to control the size and morphology of the particles through the sol gel method. The easiest way is through a hydrothermal method which requires a lower temperature compared to other methods. The interaction of the crystal seeds with the solvent molecules can tune the morphology of the active material. Generally, the electrospinning method is used to construct a one-dimensional material. The length and diameter of the particles can be varied from micrometer to nanosize by adjusting the synthesis parameters such as voltage, flow rate, molecular weight of the polymers, and concentration of the solution.[154] Controlling the morphology proves advantageous in enhancing the electrochemical performance. However, the practical application is impeded by low tap density and intricate preparation cost.[149]

https://doi.org/10.1021/acsomega.4c02709
ACS Omega 2024, 9, 22509−22531

Table 3. Overview of Different Modified Polyanionic Compounds

Strategies	Compound	Synthesis Method	Specific capacity (mA h g^{-1})	Cyclic stability	Ref
Nano structuring	Na $FePO_4$ (50 nm)	Solid state	142 at C/20	95% retention after 200 cycles at 0.05C	73
	Na_2FePO_4F (100 nm)	Solid state	116 at 0.1C	80% capacity retention after 200 cycles at 1C	119
	$Na_7V_4(P_2O_7)_4(PO_4)$ (150−200 nm)	Sol gel	116 at 0.1C	80% capacity retention after 200 cycles at 1C	155
	$Na_3(VO)_2(PO4)_2F$ (80−100 nm)	Solvothermal method	130 at 0.5C	80% capacity retention after 220 cycles at 4C	156
	$Na_3(VPO_4)_2F_3$ (50−100 nm)	Solvothermal method	110 at 0.2C	93.6% capacity retention after 200 cycles	157
	$Na_3V_2(PO_4)_2O_{1.6}F_{1.4}$ (<30 nm)	Hydrothermal synthesis	67.2 at 30C	73% capacity retention after 1000 cycles at 5C	158
	$Na_3(VO_{0.5})_2(PO_4)_2F_2$ (30 nm)	Solid state	82 at 20C	73% retention after 1000 cycles at 50C	159
	NVP@C (30 nm)	Sol−gel assisted hydrothermal method	100 at 0.5C	99.6% retention after 50 cycles at 0.5C	160
	NVP@pC (Nanoscale)	Sol gel synthesis	116.2 at 0.2C	82.1% retention after 10,000 cycles	161
Heteroatom Doping	$Na_3V_{1.95}Mg_{0.05}(PO_4)_{2.9}Cl_{0.1}$	Sol−gel	120 at 0.1C	79.4% after 30,000 cycles at 30C	162
	K^+ and Mg^{2+} codoped NVP@C/RGO	Hydrothermal	52.1 at 10C	∼95% after 500 cycles	163
	$Na_{3.01}V_{1.99}Co_{0.01}(PO_4)_3$/C	Sol gel	116 at 0.5C	80% after 1000 cycles	164
	$Na_{3-x}V_{2-x}Ti_x(PO_4)_3$/C	Solid-State	101.2 at 10C	60% after 2000 cycles at 10C	165
	$Na_3V_{1.7}Mn_{0.3}(PO_4)_3$/C	Sol gel	104 at C/2		166
	$Na_3V_{1.98}Al_{0.02}(PO_4)_3$/C	Carbon thermal reduction	102.7 at 10C	99.2% after 50 cycles	167
	$Na_3V_{2-x}Zr_x(PO_4)_{3-x}(SiO_4)_x$/C	Solid state	109.6 at 0.1C	87.7% at 6C after 500 cycles	168
	$Na_3V_{1.98}(PO_4)_{3-x}F_{3x}$/C	Solid state	143.5 at 1C	89.3% after 100 cycles	169
	$Na_3V_{1.96}Ce_{0.04}(PO_4)_3$/C	Sol gel	118 at 0.2C	99% at 10C after 100 cycles	170
Morphology controls	NVP@NSC	Solid state	113 at 1C	82.1% at 50C after 5000 cycles	171
	MNVP@C NWs	Electrospinning	78.8 at 100C	84.1% after 3000 cycles	172
	$Na_{2.97}V_{2.99}W_{0.019}(PO_4)_3$/C@CNTs	Sol gel	112.5 at 5C	86% over 500 cycles	173
	$Na_{2.9}V_{1.9}Zr_{0.1}(PO_4)_3$/C@rGO	Sol gel	81.3 at 120C	74.3% at 200C after 3000 cycles	174
	$K_{0.24}Na_{2.76}Fe_2(PO_4)_3$	Solid state	101.3 at 10C	96.5% after 500 cycles	175
	$Na_3V_{2-x}Zr_x(PO_4)_2F_3$/NC	Sol gel	98.1 at 20C	90.2% in 1000 cycles at 20C	176
	$Na_3V_{2-y}Ti_y(PO_4)_2F_3$/C	Solid state	104 at 40C	91.3% after 500 cycles at 40C	177
	$Na_3V_{1.9}Y_{0.1}(PO_4)_3$/C	Sol gel	80 at 50C	93.46% at 1C after 200 cycles	178
	Flower like NVP@C-BN	Wet-chemical method	84 at 100C	100% after 1000 cycles at 50C	178
	Highly porous-NVP@SC	Sol gel	95 at 30C	91% after 2500 cycles at 20C	82
	$Na_3V_2(PO_4)_3$@C microspheres	Membrane Casting method	96 at 30C	90% after 500 cycles at 50C	179
	NaVPO4F/C Nanofiber	electrospinning	61.2 at 50C	96.5% after 1000 cycles at 2C	180
	NVPF-gel/rGO	Hydrothermal	90.6 at 5C	86.4% after 200 cycles at 0.2C	181
	$Na_3V_2(PO_4)_2F_3$−SWCNT	Solvothermal	117 at 0.5C	92.4% after 100 cycles	182
	$Na_3V_2(PO_4)_3$/C nanoplate	Hydrothermal	76.5 at 100C	82.6% after 10,000 cycles at 50C	183

3.4. Heteroatom Doping. Cation and anion doping play a significant role in enhancing the intrinsic conductivity of the polyanionic materials by tailoring the crystallography and the electronic environment. An overview of different modified polyanionic compounds and their electrochemical performannce is given in (Table 3). Surface coating can improve surface conductivity by forming a conductive layer on the surface. Particle size reduction gives a shorter pathway for transport of ions and electrons, but it increases electrode−electrolyte contact area resulting in no beneficiary effect on intrinsic conductivity. Therefore, doping is an effective way to improve intrinsic conductivity.[184] Doping in the lattice site with aliovalent ions such as Ca, Al, and Ti will generate donor/acceptor doping effect by lowering the band gap thus improving the conductivity. Doping in the sodium site with atoms serves as a functional pillar by enlarging ion diffusion channels and by occupying structural distortion during charging−discharging. Introducing anions with higher electronegativity provides higher energy density by making use of higher potentials due to their inductive effect.[185] K,[186] Mg,[187] Li,[184] and Ca[188] are reported as dopants in the alkali sites to enhance electrochemical performance. Zheng successfully demonstrated that an increased specific capacitance can be achieved in $Na_3V_2(PO_4)_3$ by doping with Li, as the occupation of Li in the Na2 sites activates the extraction of more sodium ions during charging.[184] A similar study of Li doping in the sodium sites of $Na_3V_2(PO_4)_2O_2F$ was conducted by Liu et al., and it was observed t that the enhanced electronic and ionic conductivity is due to the increased mobile electron density and the sodium vacancies.[189]

Atomically dispersed K ions in the alkali site act as functional pillars which stabilize the structure by suppressing the unwanted phase transition during the extraction/insertion of the sodium ions, which improves the cyclic stability. The schematic illustration of K^+ ions in the sodium sites is given in Figure 8(e). Also the higher ionic radii of K^+ ions (1.38 Å) compared to Na^+ ions (1.02 Å) expands the Na-ion diffusion channels, which improves conductivity.[143] Cao et al. reported K-doped $Na_3Fe_2(Po_4)_3$ synthesized via a facile solid-state method which shows a discharge capacity of 101.3 mA h g^{-1}, which is almost

https://doi.org/10.1021/acsomega.4c02709
ACS Omega 2024, 9, 22509−22531

97% of the theoretical capacity, and the Coulombic efficiency is 100% during all the cycles.

The improved electrochemical performance of the doped one compared to the pristine material is due to the larger lattice spaces and increased diffusion coefficient of sodium ions.[175] Fang Li developed $Na_{0.84}Ca_{0.08}Fe_2PO_4(SO_4)_2$, which shows higher electrochemical performance as Ca doping in the sodium sites enhanced sodium ion diffusion kinetics, similar in the case of K-ion doping.[190] Puspitasari et al.[191] have studied the effect of Ca doping in V^{3+} sites of NVPF and found the optimal level of Ca doping at 0.05, which exhibits a specific capacity of 124 mA h g^{-1} at 0.1C and a capacity retention of 70% after 1000 cycles at 10C. The enhanced electrochemical performance was attributed to the expanded lattice spacing due to the larger ionic radii of Ca ion, which improves the diffusion kinetics of Na ion. Ca doping also reduces the bond length and strengthens the V−O and P−O bonds, thus stabilizing the oxygen atom in the structure, thus increasing the structural stability of the material. DFT studies show that doping Ca in to the V sites narrows the band gap and increases the electronic conductivity.

Doping in the transition metal sites by elements such as Cr,[192] Mn,[193] Ca,[194] Mg,[195] Fe,[196] Cu,[197] Co,[198] Al,[199] and Ti[165] has been found to improve the energy density, cyclic stability, and ionic mobility. Chen et al.[200] doped Cr in VO_6 octahedra of $Na_3V_2(PO_4)_3$ ($Na_3V_{1.5}Cr_{0.5}(PO_4)_3$), which resulted in increased energy density even in comparison with the Prussian blue analogues and the layered oxides by activating a mutielectron redox reaction at higher voltage. Cr doping activated the V^{4+}/V^{5+} redox couple, facilitating a three-electron redox couple in V and extracting the third sodium during charging in nonaqueous electrolyte in 4.2−1 V range, ultimately enhancing the energy density. Further, through DFT studies it is confirmed that an unpaired electron in the 3d orbital of Cr has improved adjacent sodium ion diffusion; thus, ionic conductivity is increased. Li et al.[201] added Cr and Si to NVP forming a multielement compound of $Na_3V_{1.9}Cr_{0.1}(PO4)_{2.9}(SiO4)_{0.1}$ (NVP-CS). A similar conclusion was drawn by Chen et al.[202] It is established that unpaired 3d electrons of Cr trigger V^{4+}/V^{5+} reaction, thereby increasing the average potential. It is found that nonreacting Cr increases the material stability, confirmed with the negative formation energy of the NVP-Cr compound. Si in the system is found to alter the electronic energy levels of V and O which aid the redox reaction of V by reducing the band gap. Due to the combined effect Cr and Si, NVP-CS has a lower migration barrier (0.073 eV) in comparison with NVP (0.144 eV). NVP-CS has attained an energy density of 357.6 W h kg^{-1} and a cyclic stability of 90% after 300 cycles at 1C.

Paek et al. have improved the sodium storage performance in $Na_3V_2(PO_4)_3$ and in $Na_3V_2(PO_4)_2F_3$ by 8.9% of Fe doping in the V sites. It is found that Fe doping makes complete use of the V^{3+}/V^{4+} redox pair and also enables the two phase transitions in $Na_3V_2(PO_4)_3$ which increase the ion diffusivity. Fe also reduces the band gap and increases the electron transport kinetics which overall resulted in long cycle life and improved energy density of the materials.[203] Similarly, Zhan et al. synthesized $Na_3V_{1.5}Fe_{.5}(PO_4)_3$@C, which shows a cyclic stability of 77.7% after 5000 cycles at 20C.[204]

Liu et al. modified $Na_4Co_3(PO_4)_2P_2O_7$ with Al doping ($Na_{3.85}Co_{2.85}Al_{0.15}(PO_4)_2P_2O_7$), which delivers a discharge capacity of 99.5 mA h g^{-1} at 0.5C and cyclic stability of 96.3% after 900 cycles at 10C. The extra vacancies created due to Al^{3+} compared to Co^{2+} improve the ionic transportation. Doping Al not only improves the ionic and electronic conductivity but also improves the structural stability of the material. Similar to cation doping, anions can also be introduced in the lattice polyanionic structure for improved electrochemical kinetics and structural stability.

Liu et al.[205] doped the PO_4^{3-} group in $Na_4Fe_3(PO_4)_2P_2O_7$ with SiO_4^{4-} achieving a specific capacity of 119.4 mA h g^{-1} at 0.1C with a capacity retention of 84.2% after 5000 cycles. This increased electrochemical performance is due to the broadened sodium ion diffusion channel which improves the ion transport. The stronger Si−O bond improves the crystal structure stability and also accommodates the volume change during charging and discharging, which in turn improves the cyclic performance. In addition, the presence of the SiO_4^{4-} group reduces the bandgap and increases the electronic conduction.

4. CONCLUSION

There has been extensive progress in the development of polyanionic materials, and among the total publications regarding SIBs, 40% is taken up by polyanionic cathodes in the past decade of SIB. They are widely explored due to their structural advantages and high voltages provided by their anionic groups. However, they are still hindered by limited energy and power densities and by poor rate capability. Herein we mainly discuss about the different strategies such as Nanostructuring, Morphology control, Surface coating, and Heteroatom doping in polyanionic cathodes for improved electrochemical performance. Reducing the particle size shortens the ion diffusion pathways and thus improves the transport kinetics of the material. A thin surface coating provides a carbon conductive surface to the material thereby improving the electronic conductivity and further enhancing the rate capability. Along with that it acts as a protective layer, which shields the active surface from electrolyte attack and in turn improves the cyclic stability of the material. Different types of morphology attained using a different synthesis process also affect the electrochemical performance of the material. Polyanionic materials are found in different architectural shapes, such as nanoflower, nanorod, porous, honeycomb, nanofiber, etc., which provide multichannel electron diffusion pathways, thus enhancing the rate capability of the material. Heteroatom doping is one of the widely explored areas as it can improve the intrinsic electronic conductivity and also contribute to the structural stability of the material which in turn enhances the cyclic performance. The type of dopant and the amount of doping should be properly optimized because doping with inert elements can result in lower energy density and also excessive doping can result in lowering the cyclic performance. Employing two or more strategies together results in enhanced electrochemical performance. These strategies contribute to sodium ion diffusion in the bulk besides improving the electronic conductivity. This work summarizes different strategies which can be used to tailor polyanionic cathode materials toward high capacity, energy density, and cyclic performance.

■ ASSOCIATED CONTENT

Supporting Information

The Supporting Information is available free of charge at https://pubs.acs.org/doi/10.1021/acsomega.4c02709.

Additional examples of surface coated materials; electrochemical performance

Table for advantages and disadvantages of sodium ion battery (PDF)

https://doi.org/10.1021/acsomega.4c02709
ACS Omega 2024, 9, 22509−22531

AUTHOR INFORMATION

Corresponding Author

Ganesh Chandra Nayak − *Department of Chemistry and Chemical Biology, Indian Institute of Technology (ISM), Dhanbad 826004 Jharkhand, India;* orcid.org/0000-0003-4470-9268; Email: gcnayak@iitism.ac.in

Authors

Anupama Joy − *Department of Chemistry and Chemical Biology, Indian Institute of Technology (ISM), Dhanbad 826004 Jharkhand, India*

Khusboo Kumari − *Department of Chemistry and Chemical Biology, Indian Institute of Technology (ISM), Dhanbad 826004 Jharkhand, India*

Fatma Parween − *Department of Chemistry and Chemical Biology, Indian Institute of Technology (ISM), Dhanbad 826004 Jharkhand, India*

Mst Shubnur Sultana − *Department of Chemistry and Chemical Biology, Indian Institute of Technology (ISM), Dhanbad 826004 Jharkhand, India*

Complete contact information is available at: https://pubs.acs.org/10.1021/acsomega.4c02709

Notes

The authors declare no competing financial interest.

ACKNOWLEDGMENTS

The authors are thankful to IIT(ISM), Dhanbad, for providing research facilities and funding.

REFERENCES

(1) Wang, G.; Zhang, L.; Zhang, J. A review of electrode materials for electrochemical supercapacitors. *Chem. Soc. Rev.* **2012**, *41* (2), 797−828.

(2) Hosaka, T.; Kubota, K.; Hameed, A. S.; Komaba, S. Research Development on K-Ion Batteries. *Chem. Rev.* **2020**, *120* (14), 6358−6466.

(3) Kar, M.; Simons, T. J.; Forsyth, M.; MacFarlane, D. R. Ionic liquid electrolytes as a platform for rechargeable metal−air batteries: a perspective. *Phys. Chem. Chem. Phys.* **2014**, *16* (35), 18658−18674.

(4) Etacheri, V.; Marom, R.; Elazari, R.; Salitra, G.; Aurbach, D. Challenges in the development of advanced Li-ion batteries: a review. *Energy Environ. Sci.* **2011**, *4* (9), 3243−3262.

(5) Dai, Z.; Mani, U.; Tan, H. T.; Yan, Q. Advanced Cathode Materials for Sodium-Ion Batteries: What Determines Our Choices? *Small Methods* **2017**, *1* (5), No. 1700098.

(6) Yabuuchi, N.; Kubota, K.; Dahbi, M.; Komaba, S. Research Development on Sodium-Ion Batteries. *Chem. Rev.* **2014**, *114* (23), 11636−11682.

(7) Zhang, H.; Tan, X.; Li, H.; Passerini, S.; Huang, W. Assessment and progress of polyanionic cathodes in aqueous sodium batteries. *Energy Environ. Sci.* **2021**, *14* (11), 5788−5800.

(8) Slater, M. D.; Kim, D.; Lee, E.; Johnson, C. S. Sodium-Ion Batteries. *Adv Funct Materials* **2013**, *23* (8), 947−958.

(9) Lyu, P.; Liu, X.; Qu, J.; Zhao, J.; Huo, Y.; Qu, Z.; Rao, Z. Recent advances of thermal safety of lithium ion battery for energy storage. *Energy Storage Materials* **2020**, *31*, 195−220.

(10) Liu, Z.; Huang, Y.; Huang, Y.; Yang, Q.; Li, X.; Huang, Z.; Zhi, C. Voltage issue of aqueous rechargeable metal-ion batteries. *Chem. Soc. Rev.* **2020**, *49* (1), 180−232.

(11) Chayambuka, K.; Mulder, G.; Danilov, D. L.; Notten, P. H. L. From Li-Ion Batteries toward Na-Ion Chemistries: Challenges and Opportunities. *Advanced Energy Materials* **2020**, *10* (38), No. 2001310.

(12) Fang, Y.; Xiao, L.; Ai, X.; Cao, Y.; Yang, H. Hierarchical Carbon Framework Wrapped $Na_3V_2(PO_4)_3$ as a Superior High-Rate and Extended Lifespan Cathode for Sodium-Ion Batteries. *Advanced Materials* **2015**, *27* (39), 5895−5900.

(13) Dai, Z.; Mani, U.; Tan, H. T.; Yan, Q. Advanced Cathode Materials for Sodium-Ion Batteries: What Determines Our Choices? *Small Methods* **2017**, *1* (5), 1700098.

(14) Yabuuchi, N.; Kubota, K.; Dahbi, M.; Komaba, S. Research Development on Sodium-Ion Batteries. *Chem. Rev.* **2014**, *114* (23), 11636−11682.

(15) Chayambuka, K.; Mulder, G.; Danilov, D. L.; Notten, P. H. From Li-ion batteries toward Na-ion chemistries: challenges and opportunities. *Advanced Energy Materials* **2020**, *10* (38), 2001310.

(16) Liu, Q.; Hu, Z.; Chen, M.; Zou, C.; Jin, H.; Wang, S.; Chou, S.-L.; Dou, S.-X. Recent Progress of Layered Transition Metal Oxide Cathodes for Sodium-Ion Batteries. *Small* **2019**, *15* (32), No. 1805381.

(17) Nayak, P. K.; Yang, L.; Brehm, W.; Adelhelm, P. From Lithium-Ion to Sodium-Ion Batteries: Advantages, Challenges, and Surprises. *Angew Chem Int Ed* **2018**, *57* (1), 102−120.

(18) Fang, C.; Huang, Y.; Zhang, W.; Han, J.; Deng, Z.; Cao, Y.; Yang, H. Routes to High Energy Cathodes of Sodium-Ion Batteries. *Advanced Energy Materials* **2016**, *6* (5), No. 1501727.

(19) Guo, J.-Z.; Gu, Z.-Y.; Du, M.; Zhao, X.-X.; Wang, X.-T.; Wu, X.-L. Emerging characterization techniques for delving polyanion-type cathode materials of sodium-ion batteries. *Mater. Today* **2023**, *66*, 221−244.

(20) Li, H.; Xu, M.; Zhang, Z.; Lai, Y.; Ma, J. Engineering of Polyanion Type Cathode Materials for Sodium-Ion Batteries: Toward Higher Energy/Power Density. *Adv Funct Materials* **2020**, *30* (28), No. 2000473.

(21) Sayahpour, B.; Hirsh, H.; Parab, S.; Nguyen, L. H. B.; Zhang, M.; Meng, Y. S. Perspective: Design of cathode materials for sustainable sodium-ion batteries. *MRS Energy & Sustainability* **2022**, *9* (2), 183−197. Sapra, S. K.; Pati, J.; Dwivedi, P. K.; Basu, S.; Chang, J.-K.; Dhaka, R. S. A comprehensive review on recent advances of polyanionic cathode materials in Na-ion batteries for cost effective energy storage applications. *WIREs Energy & Environment* **2021**, *10* (5), e400.

(22) Kim, H. Sodium-Ion Battery: Can It Compete with Li-Ion? *ACS Materials Au* **2023**, *3* (6), 571−575.

(23) Ni, Q.; Bai, Y.; Wu, F.; Wu, C. Polyanion-Type Electrode Materials for Sodium-Ion Batteries. *Advanced Science* **2017**, *4* (3), No. 1600275.

(24) Xu, C.; Zhao, J.; Yang, C.; Hu, Y.-S. Polyanionic Cathode Materials for Practical Na-Ion Batteries toward High Energy Density and Long Cycle Life. *ACS Central Science* **2023**, *9* (9), 1721−1736.

(25) Jin, T.; Li, H.; Zhu, K.; Wang, P.-F.; Liu, P.; Jiao, L. Polyanion-type cathode materials for sodium-ion batteries. *Chem. Soc. Rev.* **2020**, *49* (8), 2342−2377.

(26) Zhao, L. N.; Zhang, T.; Zhao, H. L.; Hou, Y. L. Polyanion-type electrode materials for advanced sodium-ion batteries. *Materials Today Nano* **2020**, *10*, No. 100072.

(27) Barpanda, P.; Lander, L.; Nishimura, S.-i.; Yamada, A. Polyanionic Insertion Materials for Sodium-Ion Batteries. *Advanced Energy Materials* **2018**, *8* (17), No. 1703055.

(28) Ling, J.; Karuppiah, C.; Krishnan, S. G.; Reddy, M. V.; Misnon, I. I.; Ab Rahim, M. H.; Yang, C.-C.; Jose, R. Phosphate Polyanion Materials as High-Voltage Lithium-Ion Battery Cathode: A Review. *Energy Fuels* **2021**, *35* (13), 10428−10450.

(29) Pan, H.; Hu, Y.-S.; Chen, L. Room-temperature stationary sodium-ion batteries for large-scale electric energy storage. *Energy Environ. Sci.* **2013**, *6* (8), 2338−2360.

(30) Delmas, C.; Fouassier, C.; Hagenmuller, P. Structural classification and properties of the layered oxides. *Physica B+C* **1980**, *99* (1), 81−85.

(31) Han, M. H.; Gonzalo, E.; Singh, G.; Rojo, T. A comprehensive review of sodium layered oxides: powerful cathodes for Na-ion batteries. *Energy Environ. Sci.* **2015**, *8* (1), 81−102.

(32) Komaba, S.; Yabuuchi, N.; Nakayama, T.; Ogata, A.; Ishikawa, T.; Nakai, I. Study on the reversible electrode reaction of $Na_{1-x}Ni_{0.5}Mn_{0.5}O_2$ for a rechargeable sodium-ion battery. *Inorganic chemistry* **2012**, *51* (11), 6211−6220.

(33) Dai, Z.; Mani, U.; Tan, H. T.; Yan, Q. Advanced Cathode Materials for Sodium-Ion Batteries: What Determines Our Choices? *Small Methods* **2017**, *1*, No. 1700098.
(34) Ramasamy, H. V.; Kaliyappan, K.; Thangavel, R.; Seong, W. M.; Kang, K.; Chen, Z.; Lee, Y.-S. Efficient Method of Designing Stable Layered Cathode Material for Sodium Ion Batteries Using Aluminum Doping. *J. Phys. Chem. Lett.* **2017**, *8* (20), 5021−5030.
(35) Lavela, P.; Leyva, J.; Tirado, J. L. Sustainable, low Ni-containing Mg-doped layered oxides as cathodes for sodium-ion batteries. *Dalton Transactions* **2023**, *52* (46), 17289−17298.
(36) Yuan, T.; Li, S.; Sun, Y.; Wang, J.-H.; Chen, A.-J.; Zheng, Q.; Zhang, Y.; Chen, L.; Nam, G.; Che, H.; et al. A High-Rate, Durable Cathode for Sodium-Ion Batteries: Sb-Doped O_3-Type Ni/Mn-Based Layered Oxides. *ACS Nano* **2022**, *16* (11), 18058−18070.
(37) Wang, L.; Sun, Y.-G.; Hu, L.-L.; Piao, J.-Y.; Guo, J.; Manthiram, A.; Ma, J.; Cao, A.-M. Copper-substituted $Na_{0.67}Ni_{0.3-x}Cu_xMn_{0.7}O_2$ cathode materials for sodium-ion batteries with suppressed P2−O2 phase transition. *J. Mater. Chem. A* **2017**, *5* (18), 8752−8761.
(38) Yang, Q.; Wang, P.-F.; Guo, J.-Z.; Chen, Z.-M.; Pang, W.-L.; Huang, K.-C.; Guo, Y.-G.; Wu, X.-L.; Zhang, J.-P. Advanced P2-$Na_{2/3}Ni_{1/3}Mn_{7/12}Fe_{1/12}O_2$ Cathode Material with Suppressed P2−O2 Phase Transition toward High-Performance Sodium-Ion Battery. *ACS Appl. Mater. Interfaces* **2018**, *10* (40), 34272−34282.
(39) Martinez De Ilarduya, J.; Otaegui, L.; Lopez del Amo, J. M.; Armand, M.; Singh, G. NaN_3 addition, a strategy to overcome the problem of sodium deficiency in P2-$Na_{0.67}[Fe_{0.5}Mn_{0.5}]O_2$ cathode for sodium-ion battery. *Journal of Power Sources* **2017**, *337*, 197−203.
(40) Dugas, R.; Zhang, B.; Rozier, P.; Tarascon, J. M. Optimization of Na-Ion Battery Systems Based on Polyanionic or Layered Positive Electrodes and Carbon Anodes. *J. Electrochem. Soc.* **2016**, *163* (6), A867.
(41) Wang, P.-F.; You, Y.; Yin, Y.-X.; Guo, Y.-G. Layered Oxide Cathodes for Sodium-Ion Batteries: Phase Transition, Air Stability, and Performance. *Advanced Energy Materials* **2018**, *8* (8), No. 1701912.
(42) Feng, J.; Luo, S. -h.; Wang, J.; Li, P.; Yan, S.; Li, J.; Hou, P.-q.; Wang, Q.; Zhang, Y.; Liu, X. Stable Electrochemical Properties of Magnesium-Doped Co-Free Layered P2-Type $Na_{0.67}Ni_{0.33}Mn_{0.67}O_2$ Cathode Material for Sodium Ion Batteries. *ACS Sustainable Chem. Eng.* **2022**, *10* (15), 4994−5004.
(43) Wu, X.; Guo, J.; Wang, D.; Zhong, G.; McDonald, M. J.; Yang, Y. P2-type $Na_{0.66}Ni_{0.33-x}Zn_xMn_{0.67}O_2$ as new high-voltage cathode materials for sodium-ion batteries. *J. Power Sources* **2015**, *281*, 18−26.
(44) Zhang, B.; Dugas, R.; Rousse, G.; Rozier, P.; Abakumov, A. M.; Tarascon, J.-M. Insertion compounds and composites made by ball milling for advanced sodium-ion batteries. *Nat. Commun.* **2016**, *7* (1), No. 10308.
(45) Martinez De Ilarduya, J.; Otaegui, L.; López del Amo, J. M.; Armand, M.; Singh, G. NaN_3 addition, a strategy to overcome the problem of sodium deficiency in P2-$Na_{0.67}[Fe_{0.5}Mn_{0.5}]O_2$ cathode for sodium-ion battery. *J. Power Sources* **2017**, *337*, 197−203.
(46) Do, J.; Kim, I.; Kim, H.; Jung, Y. Towards stable Na-rich layered transition metal oxides for high energy density sodium-ion batteries. *Energy Storage Materials* **2020**, *25*, 62−69.
(47) Xue, L.; Bao, S.; Yan, L.; Zhang, Y.; Lu, J.; Yin, Y. MgO-coated layered cathode oxide with enhanced stability for sodium-ion batteries. *Front. Energy Res.* **2022**, *10*, 847818.
(48) Rong, X.; Hu, E.; Lu, Y.; Meng, F.; Zhao, C.; Wang, X.; Zhang, Q.; Yu, X.; Gu, L.; Hu, Y.-S.; Li, H.; Huang, X.; Yang, X.-Q.; Delmas, C.; Chen, L. Anionic redox reaction-induced high-capacity and low-strain cathode with suppressed phase transition. *Joule* **2019**, *3* (2), 503−517.
(49) Wang, J.-z.; Teng, Y.-x.; Su, G.-q.; Bao, S.; Lu, J. A dual-modification strategy for P2-type layered oxide via bulk Mg/Ti co-substitution and MgO surface coating for sodium ion batteries. *Journal of Colloid and Interface Science* **2022**, *608*, 3013−3021. Jo, J. H.; Choi, J. U.; Konarov, A.; Yashiro, H.; Yuan, S.; Shi, L.; Sun, Y. K.; Myung, S. T. Sodium-ion batteries: building effective layered cathode materials with long-term cycling by modifying the surface via sodium phosphate. *Adv Funct Materials* **2018**, *28* (14), 1705968. Chen, T.; Ouyang, B.; Fan, X.; Zhou, W.; Liu, W.; Liu, K. J. C. E. Oxide cathodes for sodium-ion batteries: Designs, challenges, and perspectives. *Carbon Energy* **2022**, *4* (2), 170−199.
(50) Kim, H.; Kim, H.; Ding, Z.; Lee, M. H.; Lim, K.; Yoon, G.; Kang, K. Recent Progress in Electrode Materials for Sodium-Ion Batteries. *Advanced Energy Materials* **2016**, *6* (19), No. 1600943.
(51) Xiang, X.; Zhang, K.; Chen, J. Recent Advances and Prospects of Cathode Materials for Sodium-Ion Batteries. *Advanced Materials* **2015**, *27* (36), 5343−5364.
(52) Zhang, B.; Dugas, R.; Rousse, G.; Rozier, P.; Abakumov, A. M.; Tarascon, J.-M. Insertion compounds and composites made by ball milling for advanced sodium-ion batteries. *Nat Commun* **2016**, *7* (1), 10308.
(53) Peng, J.; Zhang, W.; Liu, Q.; Wang, J.; Chou, S.; Liu, H.; Dou, S. J. A. M. Prussian blue analogues for sodium-ion batteries: past, present, and future. *Advanced Materials* **2022**, *34* (15), 2108384.
(54) Wang, T.; Su, D.; Shanmukaraj, D.; Rojo, T.; Armand, M.; Wang, G. J. E. E.R. Electrode materials for sodium-ion batteries: considerations on crystal structures and sodium storage mechanisms. *Electrochem. Energ. Rev.* **2018**, *1*, 200−237. Xiao, J.; Li, X.; Tang, K.; Wang, D.; Long, M.; Gao, H.; Chen, W.; Liu, C.; Liu, H.; Wang, G. Recent progress of emerging cathode materials for sodium ion batteries. *Mater. Chem. Front.* **2021**, *5* (10), 3735−3764.
(55) Wang, L.; Song, J.; Qiao, R.; Wray, L. A.; Hossain, M. A.; Chuang, Y.-D.; Yang, W.; Lu, Y.; Evans, D.; Lee, J.-J.; Vail, S.; Zhao, X.; Nishijima, M.; Kakimoto, S.; Goodenough, J. B. Rhombohedral Prussian White as Cathode for Rechargeable Sodium-Ion Batteries. *J. Am. Chem. Soc.* **2015**, *137*, 2548.
(56) Song, J.; Wang, L.; Lu, Y.; Liu, J.; Guo, B.; Xiao, P.; Lee, J.-J.; Yang, X.-Q.; Henkelman, G.; Goodenough, J. B. Removal of Interstitial H_2O in Hexacyanometallates for a Superior Cathode of a Sodium-Ion Battery. *J. Am. Chem. Soc.* **2015**, *137* (7), 2658−2664. Yang, D.; Xu, J.; Liao, X.-Z.; Wang, H.; He, Y.-S.; Ma, Z.-F. Retracted Article: Prussian blue without coordinated water as a superior cathode for sodium-ion batteries. *Chem. Commun.* **2015**, *51* (38), 8181−8184.
(57) Wang, L.; Lu, Y.; Liu, J.; Xu, M.; Cheng, J.; Zhang, D.; Goodenough, J. B. A Superior Low-Cost Cathode for a Na-Ion Battery. *Angew Chem Int Ed* **2013**, *52* (7), 1964−1967.
(58) Tang, W.; Xie, Y.; Peng, F.; Yang, Y.; Feng, F.; Liao, X.-Z.; He, Y.-S.; Ma, Z.-F.; Chen, Z.; Ren, Y. Electrochemical performance of $NaFeFe(CN)_6$ prepared by solid reaction for sodium ion batteries. *J. Electrochem. Soc.* **2018**, *165* (16), A3910.
(59) Li, Y.; Guo, S. Material design and structure optimization for rechargeable lithium-sulfur batteries. *Matter* **2021**, *4* (4), 1142−1188.
(60) Qian, J.; Wu, C.; Cao, Y.; Ma, Z.; Huang, Y.; Ai, X.; Yang, H. Prussian Blue Cathode Materials for Sodium-Ion Batteries and Other Ion Batteries. *Advanced Energy Materials* **2018**, *8* (17), No. 1702619. Peng, J.; Zhang, W.; Liu, Q.; Wang, J.; Chou, S.; Liu, H.; Dou, S. Prussian Blue Analogues for Sodium-Ion Batteries: Past, Present, and Future. *Advanced Materials* **2022**, *34* (15), No. 2108384.
(61) Gong, Z.; Yang, Y. Recent advances in the research of polyanion-type cathode materials for Li-ion batteries. *Energy Environ. Sci.* **2011**, *4* (9), 3223−3242.
(62) Padhi, A. K.; Nanjundaswamy, K. S.; Masquelier, C.; Goodenough, J. B. Mapping of Transition Metal Redox Energies in Phosphates with NASICON Structure by Lithium Intercalation. *J. Electrochem. Soc.* **1997**, *144* (8), 2581.
(63) Li, M.; Lu, J.; Chen, Z.; Amine, K. 30 Years of Lithium-Ion Batteries. *Advanced Materials* **2018**, *30* (33), No. 1800561.
(64) Moreau, P.; Guyomard, D.; Gaubicher, J.; Boucher, F. Structure and Stability of Sodium Intercalated Phases in Olivine $FePO_4$. *Chem. Mater.* **2010**, *22*, 4126−4128.
(65) Moreau, P.; Guyomard, D.; Gaubicher, J.; Boucher, F. Structure and Stability of Sodium Intercalated Phases in Olivine $FePO_4$. *Chem. Mater.* **2010**, *22* (14), 4126−4128.
(66) Kim, J.; Seo, D.-H.; Kim, H.; Park, I.; Yoo, J.-K.; Jung, S.-K.; Park, Y.-U.; Goddard III, W. A.; Kang, K. Unexpected discovery of low-cost maricite $NaFePO_4$ as a high-performance electrode for Na-ion batteries. *Energy Environ. Sci.* **2015**, *8* (2), 540−545.

https://doi.org/10.1021/acsomega.4c02709
ACS Omega 2024, 9, 22509−22531

(67) Fernández-Ropero, A. J.; Saurel, D.; Acebedo, B.; Rojo, T.; Casas-Cabanas, M. Electrochemical characterization of $NaFePO_4$ as positive electrode in aqueous sodium-ion batteries. *J. Power Sources* **2015**, *291*, 40−45.
(68) Oh, S.-M.; Myung, S.-T.; Hassoun, J.; Scrosati, B.; Sun, Y.-K. Reversible $NaFePO_4$ electrode for sodium secondary batteries. *Electrochemistry Communications* **2012**, *22*, 149−152.
(69) Avdeev, M.; Mohamed, Z.; Ling, C. D.; Lu, J.; Tamaru, M.; Yamada, A.; Barpanda, P. Magnetic Structures of $NaFePO_4$ Maricite and Triphylite Polymorphs for Sodium-Ion Batteries. *Inorganic chemistry* **2013**, *52* (15), 8685−8693.
(70) Saracibar, A.; Carrasco, J.; Saurel, D.; Galceran, M.; Acebedo, B.; Anne, H.; Lepoitevin, M.; Rojo, T.; Casas Cabanas, M. Investigation of sodium insertion−extraction in olivine Na_xFePO_4 ($0 \leq x \leq 1$) using first-principles calculations. *Phys. Chem. Chem. Phys.* **2016**, *18* (18), 13045−13051. Galceran, M.; Roddatis, V.; Zúñiga, F. J.; Pérez-Mato, J. M.; Acebedo, B.; Arenal, R.; Peral, I.; Rojo, T.; Casas-Cabanas, M. Na−Vacancy and Charge Ordering in $Na_{\approx 2/3}FePO_4$. *Chem. Mater.* **2014**, *26* (10), 3289−3294.
(71) Ali, G.; Lee, J.-H.; Susanto, D.; Choi, S.-W.; Cho, B. W.; Nam, K.-W.; Chung, K. Y. Polythiophene-Wrapped Olivine $NaFePO_4$ as a Cathode for Na-Ion Batteries. *ACS Appl. Mater. Interfaces* **2016**, *8* (24), 15422−15429.
(72) Saurel, D.; Giner, M.; Galceran, M.; Rodríguez-Carvajal, J.; Reynaud, M.; Casas-Cabanas, M. The triphylite $NaFe_{1-y}MnyPO_4$ solid solution ($0 \leq y \leq 1$): Kinetic strain accommodation in $Na_xFe_{0.8}Mn_{0.2}PO_4$. *Electrochim. Acta* **2022**, *425*, No. 140650. Henriksen, C.; Mathiesen, J. K.; Chiang, Y.-M.; Jensen, K. M. Ø.; Ravnsbæk, D. B. Reducing Transformation Strains during Na Intercalation in Olivine $FePO_4$ Cathodes by Mn Substitution. *ACS Applied Energy Materials* **2019**, *2* (11), 8060−8067. Yamada, A.; Kudo, Y.; Liu, K.-Y. Reaction mechanism of the olivine-type $Li_x(Mn_{0.6}Fe_{0.4})$-PO_4 ($0 \leqslant x \leqslant 1$). *J. Electrochem. Soc.* **2001**, *148* (7), A747. Drozhzhin, O. A.; Sumanov, V. D.; Karakulina, O. M.; Abakumov, A. M.; Hadermann, J.; Baranov, A. N.; Stevenson, K. J.; Antipov, E. V. J. E. A. Switching between solid solution and two-phase regimes in the $Li_{1-x}Fe_{1-y}MnyPO_4$ cathode materials during lithium (de) insertion: combined PITT, in situ XRPD and electron diffraction tomography study. *Electrochimica Acta* **2016**, *191*, 149−157.
(73) Kim, J.; Seo, D.-H.; Kim, H.; Park, I.; Yoo, J.-K.; Jung, S.-K.; Park, Y.-U.; Goddard, W. A., Iii; Kang, K. Unexpected discovery of low-cost maricite $NaFePO_4$ as a high-performance electrode for Na-ion batteries. *Energy Environ. Sci.* **2015**, *8* (2), 540−545.
(74) Liu, Y.; Zhang, N.; Wang, F.; Liu, X.; Jiao, L.; Fan, L.-Z. Approaching the downsizing limit of maricite $NaFePO_4$ toward high-performance cathode for sodium-ion batteries. *Adv Funct Materials* **2018**, *28* (30), 1801917. Rahman, M. M.; Sultana, I.; Mateti, S.; Liu, J.; Sharma, N.; Chen, Y. Maricite $NaFePO_4$/C/graphene: a novel hybrid cathode for sodium-ion batteries. *Journal of Materials Chemistry A* **2017**, *5* (32), 16616−16621.
(75) Boyadzhieva, T.; Koleva, V.; Stoyanova, R. Crystal chemistry of Mg substitution in $NaMnPO_4$ olivine: concentration limit and cation distribution. *Phys. Chem. Chem. Phys.* **2017**, *19* (20), 12730−12739.
(76) Anantharamulu, N. a.; Koteswara Rao, K.; Rambabu, G.; Vijaya Kumar, B.; Radha, V.; Vithal, M. A wide-ranging review on Nasicon type materials. *J Mater Sci* **2011**, *46*, 2821−2837. Liu, Y.; Li, J.; Shen, Q.; Zhang, J.; He, P.; Qu, X.; Liu, Y. Advanced characterizations and measurements for sodium-ion batteries with NASICON-type cathode materials. *eScience* **2022**, *2* (1), 10−31.
(77) Goodenough, J. B.; Hong, H. Y. P.; Kafalas, J. A. Fast Na^+-ion transport in skeleton structures. *Mater. Res. Bull.* **1976**, *11* (2), 203−220. Jian, Z.; Hu, Y.-S.; Ji, X.; Chen, W. NASICON-Structured Materials for Energy Storage. *Advanced Materials* **2017**, *29* (20), No. 1601925. Delmas, C. Sodium and Sodium-Ion Batteries: 50 Years of Research. *Advanced Energy Materials* **2018**, *8* (17), No. 1703137.
(78) Thirupathi, R.; Kumari, V.; Chakrabarty, S.; Omar, S. Recent progress and prospects of NASICON framework electrodes for Na-ion batteries. *Prog. Mater. Sci.* **2023**, *137*, No. 101128.
(79) Song, W.; Ji, X.; Wu, Z.; Zhu, Y.; Yang, Y.; Chen, J.; Jing, M.; Li, F.; Banks, C. E. First exploration of Na-ion migration pathways in the NASICON structure $Na_3V_2(PO_4)_3$. *Journal of Materials Chemistry A* **2014**, *2* (15), 5358−5362.
(80) Park, S.; Chotard, J.-N.; Carlier, D.; Moog, I.; Courty, M.; Duttine, M.; Fauth, F.; Iadecola, A.; Croguennec, L.; Masquelier, C. Crystal Structures and Local Environments of NASICON-Type $Na_3FeV(PO_4)_3$ and $Na_4FeV(PO_4)_3$ Positive Electrode Materials for Na-Ion Batteries. *Chem. Mater.* **2021**, *33* (13), 5355−5367.
(81) Zhou, Y.; Rui, X.; Sun, W.; Xu, Z.; Zhou, Y.; Ng, W. J.; Yan, Q.; Fong, E. Biochemistry-Enabled 3D Foams for Ultrafast Battery Cathodes. *ACS Nano* **2015**, *9* (4), 4628−4635.
(82) Li, W.; Yao, Z.; Zhong, Y.; Zhou, C.-a.; Wang, X.; Xia, X.; Xie, D.; Wu, J.; Gu, C.; Tu, J. Enhancement of the advanced Na storage performance of $Na_3V_2(PO_4)_3$ in a symmetric sodium full cell via a dual strategy design. *Journal of Materials Chemistry A* **2019**, *7* (17), 10231−10238.
(83) Shen, L.; Li, Y.; Roy, S.; Yin, X.; Liu, W.; Shi, S.; Wang, X.; Yin, X.; Zhang, J.; Zhao, Y. A robust carbon coating of $Na_3V_2(PO_4)_3$ cathode material for high performance sodium-ion batteries. *Chin. Chem. Lett.* **2021**, *32* (11), 3570−3574.
(84) El Aggadi, S.; Ennouhi, M.; Boutakiout, A.; El Hourch, A. Progress towards efficient phosphate-based materials for sodium-ion batteries in electrochemical energy storage. *Ionics* **2023**, *29* (6), 2099−2113.
(85) Guo, S.-P.; Li, J.-C.; Xu, Q.-T.; Ma, Z.; Xue, H.-G. Recent achievements on polyanion-type compounds for sodium-ion batteries: syntheses, crystal chemistry and electrochemical performance. *Journal of Power Sources* **2017**, *361*, 285−299.
(86) Clark, J. M.; Barpanda, P.; Yamada, A.; Islam, M. S. Sodium-ion battery cathodes $Na_2FeP_2O_7$ and $Na_2MnP_2O_7$: diffusion behaviour for high rate performance. *J. Mater. Chem. A* **2014**, *2* (30), 11807−11812.
(87) Kee, Y.; Dimov, N.; Staikov, A.; Barpanda, P.; Lu, Y.-C.; Minami, K.; Okada, S. Insight into the limited electrochemical activity of $NaVP_2O_7$. *RSC Adv.* **2015**, *5* (80), 64991−64996.
(88) Shen, B.; Xu, M.; Niu, Y.; Han, J.; Lu, S.; Jiang, J.; Li, Y.; Dai, C.; Hu, L.; Li, C. Sodium-rich ferric pyrophosphate cathode for stationary room-temperature sodium-ion batteries. *ACS Appl. Mater. Interfaces* **2018**, *10* (1), 502−508.
(89) Hwang, J.-Y.; Myung, S.-T.; Sun, Y.-K. Sodium-ion batteries: present and future. *Chem. Soc. Rev.* **2017**, *46* (12), 3529−3614. Wood, S. M.; Eames, C.; Kendrick, E.; Islam, M. S. Sodium ion diffusion and voltage trends in phosphates $Na_4M_3(PO_4)_2P_2O_7$ (M = Fe, Mn, Co, Ni) for possible high-rate cathodes. *J. Phys. Chem. C* **2015**, *119* (28), 15935−15941.
(90) Kim, H.; Park, I.; Lee, S.; Kim, H.; Park, K.-Y.; Park, Y.-U.; Kim, H.; Kim, J.; Lim, H.-D.; Yoon, W.-S.; et al. Understanding the Electrochemical Mechanism of the New Iron-Based Mixed-Phosphate $Na_4Fe_3(PO_4)_2(P_2O_7)$ in a Na Rechargeable Battery. *Chem. Mater.* **2013**, *25* (18), 3614−3622.
(91) Ye, T.; Barpanda, P.; Nishimura, S.-i.; Furuta, N.; Chung, S.-C.; Yamada, A. General observation of Fe^{3+}/Fe^{2+} redox couple close to 4 V in partially substituted $Li_2FeP_2O_7$ pyrophosphate solid-solution cathodes. *Chem. Mater.* **2013**, *25* (18), 3623−3629.
(92) Kim, H.; Yoon, G.; Park, I.; Park, K.-Y.; Lee, B.; Kim, J.; Park, Y.-U.; Jung, S.-K.; Lim, H.-D.; Ahn, D.; Lee, S.; Kang, K. Anomalous Jahn−Teller behavior in a manganese-based mixed-phosphate cathode for sodium ion batteries. *Energy Environ. Sci.* **2015**, *8* (11), 3325−3335.
(93) Kim, H.; Park, I.; Lee, S.; Kim, H.; Park, K.-Y.; Park, Y.-U.; Kim, H.; Kim, J.; Lim, H.-D.; Yoon, W.-S.; Kang, K. Understanding the electrochemical mechanism of the new iron-based mixed-phosphate $Na_4Fe_3(PO_4)_2(P_2O_7)$ in a Na rechargeable battery. *Chem. Mater.* **2013**, *25* (18), 3614−3622.
(94) Ren, W.; Qin, M.; Zhou, Y.; Zhou, H.; Zhu, J.; Pan, J.; Zhou, J.; Cao, X.; Liang, S. Electrospun $Na_4Fe_3(PO_4)_2(P_2O_7)$ nanofibers as free-standing cathodes for ultralong-life and high-rate sodium-ion batteries. *Energy Storage Materials* **2023**, *54*, 776−783.
(95) Ge, X.; Li, H.; Li, J.; Guan, C.; Wang, X.; He, L.; Li, S.; Lai, Y.; Zhang, Z. High-Entropy Doping Boosts Ion/Electronic Transport of

https://doi.org/10.1021/acsomega.4c02709
ACS Omega 2024, 9, 22509−22531

$Na_4Fe_3(PO_4)_2(P_2O_7)$/C Cathode for Superior Performance Sodium-Ion Batteries. *Small* **2023**, *19*, 2302609.
(96) Barpanda, P.; Oyama, G.; Nishimura, S.-i.; Chung, S.-C.; Yamada, A. A 3.8-V earth-abundant sodium battery electrode. *Nat Commun* **2014**, *5* (1), 4358.
(97) Gao, Y.; Zhang, H.; Liu, X. H.; Yang, Z.; He, X. X.; Li, L.; Qiao, Y.; Chou, S. L. Low-cost polyanion-type sulfate cathode for sodium-ion battery. *Advanced Energy Materials* **2021**, *11* (42), 2101751.
(98) Chakraborty, S.; Banerjee, A.; Watcharatharapong, T.; Araujo, R. B; Ahuja, R. Current computational trends in polyanionic cathode materials for Li and Na batteries. *J. Phys.: Condens. Matterl* **2018**, *30* (28), 283003.
(99) Barpanda, P. J. Sulfate Chemistry for High-Voltage Insertion Materials: Synthetic, Structural and Electrochemical Insights. *Israel Journal of Chemistry* **2015**, *55* (5), 537−557.
(100) Xu, C.; Zhao, J.; Yang, C.; Hu, Y.-S. Polyanionic Cathode Materials for Practical Na-Ion Batteries toward High Energy Density and Long Cycle Life. *ACS Cent. Sci.* **2023**, *9*, 1721−1736.
(101) Ni, Q.; Bai, Y.; Wu, F.; Wu, C. Polyanion-type electrode materials for sodium-ion batteries. *Advanced Science* **2017**, *4* (3), 1600275.
(102) Jin, T.; Li, H.; Zhu, K.; Wang, P.-F.; Liu, P.; Jiao, L. Polyanion-type cathode materials for sodium-ion batteries. *Chem. Soc. Rev.* **2020**, *49* (8), 2342−2377.
(103) Zhang, J.; Yan, Y.; Wang, X.; Cui, Y.; Zhang, Z.; Wang, S.; Xie, Z.; Yan, P.; Chen, W. Bridging multiscale interfaces for developing ionically conductive high-voltage iron sulfate-containing sodium-based battery positive electrodes. *Nat Commun* **2023**, *14* (1), 3701.
(104) Liu, X.; Tang, L.; Xu, Q.; Liu, H.; Wang, Y. Ultrafast and ultrastable high voltage cathode of $Na_{2+2x}Fe_{2-x}(SO_4)_3$ microsphere scaffolded by graphene for sodium ion batteries. *Electrochim. Acta* **2019**, *296*, 345−354.
(105) Niu, Y.; Zhao, Y.; Xu, M. Manganese-based polyanionic cathodes for sodium-ion batteries. *Carbon Neutralization* **2023**, *2* (2), 150−168.
(106) Kovrugin, V. M.; Nekrasova, D. O.; Siidra, O. I.; Mentre, O.; Masquelier, C.; Stefanovich, S. Y.; Colmont, M. Mineral-Inspired Crystal Growth and Physical Properties of $Na_2Cu(SO_4)_2$ and Review of $Na_2M(SO_4)_2(H_2O)_x$ (x = 0−6) Compounds. *Crystal Growth & Design* **2019**, *19* (2), 1233−1244.
(107) Singh, S.; Neveu, A.; Jayanthi, K.; Das, T.; Chakraborty, S.; Navrotsky, A.; Pralong, V.; Barpanda, P. J. D. T. Facile synthesis and phase stability of Cu-based $Na_2Cu(SO_4)_2{\cdot}xH_2O$ (x = 0−2) sulfate minerals as conversion type battery electrodes. *Dalton Trans.* **2022**, *51* (29), 11169−11179.
(108) Sauvage, F.; Quarez, E.; Tarascon, J.-M.; Baudrin, E. Crystal structure and electrochemical properties vs Na^+ of the sodium fluorophosphate $Na_{1.5}VOPO_4F_{0.5}$. *Solid State Sciences* **2006**, *8* (10), 1215−1221.
(109) Massa, W.; Yakubovich, O. V.; Dimitrova, O. V. J. S. s. s. Crystal structure of a new sodium vanadyl(IV) fluoride phosphate $Na_3\{V_2O_2F[PO_4]_2\}$. *Solid State Sciences* **2002**, *4* (4), 495−501.
(110) Qi, Y.; Mu, L.; Zhao, J.; Hu, Y. S.; Liu, H.; Dai, S. J. A. C. I. E. Superior Na-storage performance of low-temperature-synthesized $Na_3(VO_{1-x}PO_4)_2F_{1+2x}$ ($0 \le x \le 1$) nanoparticles for Na-ion batteries. *Angew Chem Int Ed* **2015**, *54* (34), 9911−9916.
(111) Barpanda, P.; Ati, M.; Melot, B. C.; Rousse, G.; Chotard, J. N.; Doublet, M. L.; Sougrati, M. T.; Corr, S. A.; Jumas, J. C.; Tarascon, J. M. A 3.90 V iron-based fluorosulphate material for lithium-ion batteries crystallizing in the triplite structure. *Nat. Mater.* **2011**, *10* (10), 772−779.
(112) Kim, M.; Kim, D.; Lee, W.; Jang, H.; Kang, B. New Class of 3.7 V Fe-Based Positive Electrode Materials for Na-Ion Battery Based on Cation-Disordered Polyanion Framework. *Chem. Mater.* **2018**, *30*, 6346.
(113) Chen, C.-Y.; Matsumoto, K.; Nohira, T.; Hagiwara, R. J. E.c. Na_2MnSiO_4 as a positive electrode material for sodium secondary batteries using an ionic liquid electrolyte. *Electrochemistry Communications* **2014**, *45*, 63−66.
(114) Ali, B.; ur-Rehman, A.; Ghafoor, F.; Shahzad, M. I.; Shah, S. K.; Abbas, S. M. Interconnected mesoporous Na_2FeSiO_4 nanospheres supported on carbon nanotubes as a highly stable and efficient cathode material for sodium-ion battery. *J. Power Sources* **2018**, *396*, 467−475.
(115) Masquelier, C.; Croguennec, L. J. C. R. Polyanionic (phosphates, silicates, sulfates) frameworks as electrode materials for rechargeable Li (or Na) batteries. *Chem. Rev.* **2013**, *113* (8), 6552−6591. Gummow, R.; He, Y. Recent progress in the development of Li_2MnSiO_4 cathode materials. *Journal of Power Sources* **2014**, *253*, 315−331. Islam, M. S.; Dominko, R.; Masquelier, C.; Sirisopanaporn, C.; Armstrong, A. R.; Bruce, P. G. Silicate cathodes for lithium batteries: alternatives to phosphates? *J. Mater. Chem.* **2011**, *21* (27), 9811−9818. Dominko, R.; Bele, M.; Gaberšček, M.; Meden, A.; Remškar, M.; Jamnik, J. J. E. C. Structure and electrochemical performance of Li_2MnSiO_4 and Li_2FeSiO_4 as potential Li-battery cathode materials. *Electrochemistry Communications* **2006**, *8* (2), 217−222. Dominko, R.; Bele, M.; Kokalj, A.; Gaberscek, M.; Jamnik, J. J. J. o. P. S. Li_2MnSiO_4 as a potential Li-battery cathode material. *Journal of Power Sources* **2007**, *174* (2), 457−461. Muraliganth, T.; Stroukoff, K.; Manthiram, A. J. C. o. M. Microwave-solvothermal synthesis of nanostructured Li2MSiO4/C (M = Mn and Fe) cathodes for lithium-ion batteries. *Chem. Mater.* **2010**, *22* (20), 5754−5761. Nishimura, S.-i.; Hayase, S.; Kanno, R.; Yashima, M.; Nakayama, N.; Yamada, A. Structure of Li_2FeSiO_4. *J. Am. Chem. Soc.* **2008**, *130* (40), 13212−13213. Rangappa, D.; Murukanahally, K. D.; Tomai, T.; Unemoto, A.; Honma, I. J. N. l. Ultrathin nanosheets of Li_2MSiO_4 (M = Fe, Mn) as high-capacity Li-ion battery electrode. *Nano Lett.* **2012**, *12* (3), 1146−1151.
(116) Treacher, J. C.; Wood, S. M.; Islam, M. S.; Kendrick, E. J. P. C. C. P. Na 2 CoSiO 4 as a cathode material for sodium-ion batteries: structure, electrochemistry and diffusion pathways. *Phys. Chem. Chem. Phys.* **2016**, *18* (48), 32744−32752. Zhao, X.; Wu, S.; Lv, X.; Nguyen, M. C.; Wang, C.-Z.; Lin, Z.; Zhu, Z.-Z.; Ho, K.-M. J. S. r. Exploration of tetrahedral structures in silicate cathodes using a motif-network scheme. *Sci Rep* **2015**, *5* (1), 15555. Li, S.; Guo, J.; Ye, Z.; Zhao, X.; Wu, S.; Mi, J.-X.; Wang, C.-Z.; Gong, Z.; McDonald, M. J; Zhu, Z.; Ho, K.-M.; Yang, Y. Zero-strain Na_2FeSiO_4 as novel cathode material for sodium-ion batteries. *ACS Appl. Mater. Interfaces* **2016**, *8* (27), 17233−17238.
(117) Zhao, L.; Zhao, H.; Du, Z.; Chen, N.; Chang, X.; Zhang, Z.; Gao, F.; Trenczek-Zajac, A.; Świerczek, K. Computational and experimental understanding of Al-doped $Na_3V_{2-x}Al_x(PO_4)_3$ cathode material for sodium ion batteries: Electronic structure, ion dynamics and electrochemical properties. *Electrochim. Acta* **2018**, *282*, 510−519.
(118) Zhang, H.; Huang, Y.; Ming, H.; Cao, G.; Zhang, W.; Ming, J.; Chen, R. Recent advances in nanostructured carbon for sodium-ion batteries. *Journal of Materials Chemistry A* **2020**, *8* (4), 1604−1630.
(119) Law, M.; Ramar, V.; Balaya, P. Synthesis, characterisation and enhanced electrochemical performance of nanostructured Na_2FePO_4F for sodium batteries. *RSC Adv.* **2015**, *5* (62), 50155−50164.
(120) Fang, J.; Wang, S.; Li, Z.; Chen, H.; Xia, L.; Ding, L.; Wang, H. Porous $Na_3V_2(PO_4)_3$@C nanoparticles enwrapped in three-dimensional graphene for high performance sodium-ion batteries. *Journal of Materials Chemistry A* **2016**, *4* (4), 1180−1185. Song, M.; Wang, C.; Du, D.; Li, F.; Chen, J. A high-energy-density sodium-ion full battery based on tin anode. *Science China Chemistry* **2019**, *62* (5), 616−621. Xiong, H.; Qian, R.; Liu, Z.; Zhang, R.; Sun, G.; Guo, B.; Du, F.; Song, S.; Qiao, Z. A.; Dai, S. J. A. S. A Polymer-Assisted Spinodal Decomposition Strategy toward Interconnected Porous Sodium Super Ionic Conductor-Structured Polyanion-Type Materials and Their Application as a High-Power Sodium-Ion Battery Cathode. *Advanced Science* **2021**, *8* (11), 2004943.
(121) Saravanan, K.; Mason, C. W.; Rudola, A.; Wong, K. H.; Balaya, P. The First Report on Excellent Cycling Stability and Superior Rate Capability of $Na_3V_2(PO_4)_3$ for Sodium Ion Batteries. *Advanced Energy Materials* **2013**, *3* (4), 444−450.
(122) Cao, X.; Pan, A.; Yin, B.; Fang, G.; Wang, Y.; Kong, X.; Zhu, T.; Zhou, J.; Cao, G.; Liang, S. Nanoflake-constructed porous $Na_3V_2(PO_4)_3$/C hierarchical microspheres as a bicontinuous cathode for sodium-ion batteries applications. *Nano Energy* **2019**, *60*, 312−323.

https://doi.org/10.1021/acsomega.4c02709
ACS Omega 2024, 9, 22509−22531

(123) Zheng, M.; Tang, H.; Li, L.; Hu, Q.; Zhang, L.; Xue, H.; Pang, H. Hierarchically Nanostructured Transition Metal Oxides for Lithium-Ion Batteries. *Advanced Science* **2018**, *5* (3), Review.
(124) Xu, H.; Yan, Q.; Yao, W.; Lee, C.-S.; Tang, Y. Mainstream Optimization Strategies for Cathode Materials of Sodium-Ion Batteries. *Small Structures* **2022**, *3* (4), No. 2100217.
(125) Zhang, K.; Hu, Z.; Tao, Z.; Chen, J. Inorganic & organic materials for rechargeable Li batteries with multi-electron reaction. *Science China Materials* **2014**, *57* (1), 42−58.
(126) Duan, W.; Zhu, Z.; Li, H.; Hu, Z.; Zhang, K.; Cheng, F.; Chen, J. $Na_3V_2(PO_4)_3$@C core−shell nanocomposites for rechargeable sodium-ion batteries. *Journal of Materials Chemistry A* **2014**, *2* (23), 8668−8675.
(127) Cheng, J.; Fong, K. D.; Persson, K. A. Materials design principles of amorphous cathode coatings for lithium-ion battery applications. *Journal of Materials Chemistry A* **2022**, *10* (41), 22245−22256.
(128) Li, W.-J.; Chou, S.-L.; Wang, J.-Z.; Wang, J.-L.; Gu, Q.-F.; Liu, H.-K.; Dou, S.-X. Multifunctional conducing polymer coated $Na_{1+x}MnFe(CN)_6$ cathode for sodium-ion batteries with superior performance via a facile and one-step chemistry approach. *Nano Energy* **2015**, *13*, 200−207.
(129) Zuo, D.; Tian, G.; Li, X.; Chen, D.; Shu, K. Recent progress in surface coating of cathode materials for lithium ion secondary batteries. *J. Alloys Compd.* **2017**, *706*, 24−40.
(130) Oh, S. W.; Myung, S.-T.; Oh, S.-M.; Oh, K. H.; Amine, K.; Scrosati, B.; Sun, Y.-K. Double Carbon Coating of $LiFePO_4$ as High Rate Electrode for Rechargeable Lithium Batteries. *Advanced Materials* **2010**, *22* (43), 4842−4845.
(131) Fang, Y.; Xiao, L.; Ai, X.; Cao, Y.; Yang, H. J. A. m. Hierarchical carbon framework wrapped $Na_3V_2(PO_4)_3$ as a superior high-rate and extended lifespan cathode for sodium-ion batteries. *Advanced Materials* **2015**, *27* (39), 5895−5900.
(132) Wu, X.; Zhong, G.; Yang, Y. Sol-gel synthesis of $Na_4Fe_3(PO_4)_2(P_2O_7)$/C nanocomposite for sodium ion batteries and new insights into microstructural evolution during sodium extraction. *J. Power Sources* **2016**, *327*, 666−674.
(133) Chen, X.; Du, K.; Lai, Y.; Shang, G.; Li, H.; Xiao, Z.; Chen, Y.; Li, J.; Zhang, Z. In-situ carbon-coated $Na_2FeP_2O_7$ anchored in three-dimensional reduced graphene oxide framework as a durable and high-rate sodium-ion battery cathode. *J. Power Sources* **2017**, *357*, 164−172.
(134) Ling, R.; Cai, S.; Shen, K.; Sang, Z.; Xie, D.; Sun, J.; Xiong, K.; Guo, J.; Sun, X. Dual carbon-confined Na_2MnPO_4F nanoparticles as a superior cathode for rechargeable sodium-ion battery. *Ceram. Int.* **2019**, *45* (16), 19799−19807.
(135) Deng, X.; Shi, W.; Sunarso, J.; Liu, M.; Shao, Z. A Green Route to a Na_2FePO_4F-Based Cathode for Sodium Ion Batteries of High Rate and Long Cycling Life. *ACS Appl. Mater. Interfaces* **2017**, *9* (19), 16280−16287.
(136) Chen, L.; Zhao, Y.; Liu, S.; Zhao, L. Hard Carbon Wrapped $Na_3V_2(PO_4)_3$@C Porous Composite Extending Cycling Lifespan for Sodium-Ion Batteries. *ACS Appl. Mater. Interfaces* **2017**, *9* (51), 44485−44493.
(137) Chen, H.; Zhang, B.; Wang, X.; Dong, P.; Tong, H.; Zheng, J.-c.; Yu, W.; Zhang, J. CNT-Decorated $Na_3V_2(PO_4)_3$ Microspheres as a High-Rate and Cycle-Stable Cathode Material for Sodium Ion Batteries. *ACS Appl. Mater. Interfaces* **2018**, *10* (4), 3590−3595.
(138) Tang, L.; Liu, X.; Li, Z.; Pu, X.; Zhang, J.; Xu, Q.; Liu, H.; Wang, Y.-G.; Xia, Y. CNT-Decorated $Na_4Mn_2Co(PO_4)_2P_2O_7$ Microspheres as a Novel High-Voltage Cathode Material for Sodium-Ion Batteries. *ACS Appl. Mater. Interfaces* **2019**, *11* (31), 27813−27822.
(139) Feng, Z.; Tang, M.; Yan, Z. 3D conductive CNTs anchored with Na_2FeSiO_4 nanocrystals as a novel cathode material for electrochemical sodium storage. *Ceram. Int.* **2018**, *44* (17), 22019−22022.
(140) Rui, X.; Sun, W.; Wu, C.; Yu, Y.; Yan, Q. An Advanced Sodium-Ion Battery Composed of Carbon Coated $Na_3V_2(PO_4)_3$ in a Porous Graphene Network. *Advanced Materials* **2015**, *27* (42), 6670−6676.
(141) Ling, R.; Cai, S.; Shen, S.; Hu, X.; Xie, D.; Zhang, F.; Sun, X.; Yu, N.; Wang, F. Synthesis of carbon coated Na_2FePO_4F as cathode materials for high-performance sodium ion batteries. *J. Alloys Compd.* **2017**, *704*, 631−640.
(142) Zhu, C.; Song, K.; van Aken, P. A.; Maier, J.; Yu, Y. Carbon-Coated $Na_3V_2(PO_4)_3$ Embedded in Porous Carbon Matrix: An Ultrafast Na-Storage Cathode with the Potential of Outperforming Li Cathodes. *Nano Lett.* **2014**, *14* (4), 2175−2180.
(143) Lim, S.-J.; Han, D.-W.; Nam, D.-H.; Hong, K.-S.; Eom, J.-Y.; Ryu, W.-H.; Kwon, H.-S. Structural enhancement of $Na_3V_2(PO_4)_3$/C composite cathode materials by pillar ion doping for high power and long cycle life sodium-ion batteries. *Journal of Materials Chemistry A* **2014**, *2* (46), 19623−19632.
(144) Klee, R.; Wiatrowski, M.; Aragón, M. J.; Lavela, P.; Ortiz, G. F.; Alcántara, R.; Tirado, J. L. Improved Surface Stability of C+M_xO_y@$Na_3V_2(PO_4)_3$ Prepared by Ultrasonic Method as Cathode for Sodium-Ion Batteries. *ACS Appl. Mater. Interfaces* **2017**, *9* (2), 1471−1478.
(145) Liu, J.; Tang, K.; Song, K.; van Aken, P. A.; Yu, Y.; Maier, J. J. N. Electrospun $Na_3V_2(PO_4)_3$/C nanofibers as stable cathode materials for sodium-ion batteries. *Nanoscale* **2014**, *6* (10), 5081−5086. Mai, L.; Tian, X.; Xu, X.; Chang, L.; Xu, L. Nanowire Electrodes for Electrochemical Energy Storage Devices. *Chem. Rev.* **2014**, *114* (23), 11828−11862.
(146) Ren, W.; Zheng, Z.; Xu, C.; Niu, C.; Wei, Q.; An, Q.; Zhao, K.; Yan, M.; Qin, M.; Mai, L. Self-sacrificed synthesis of three-dimensional $Na_3V_2(PO_4)_3$ nanofiber network for high-rate sodium−ion full batteries. *Nano Energy* **2016**, *25*, 145−153.
(147) Meng, Y.; Zhang, S.; Deng, C. Superior sodium−lithium intercalation and depressed moisture sensitivity of a hierarchical sandwich-type nanostructure for a graphene−sulfate composite: a case study on $Na_2Fe(SO_4)_2{\cdot}2H_2O$. *Journal of Materials Chemistry A* **2015**, *3* (8), 4484−4492.
(148) Anwer, S.; Huang, Y.; liu, J.; Liu, J.; Xu, M.; Wang, Z.; Chen, R.; Zhang, J.; Wu, F. Nature-Inspired Na2Ti3O7 Nanosheets-Formed Three-Dimensional Microflowers Architecture as a High-Performance Anode Material for Rechargeable Sodium-Ion Batteries. *ACS Appl. Mater. Interfaces* **2017**, *9* (13), 11669−11677.
(149) Xiong, H.; Sun, G.; Liu, Z.; Zhang, L.; Li, L.; Zhang, W.; Du, F.; Qiao, Z.-A. Polymer Stabilized Droplet Templating towards Tunable Hierarchical Porosity in Single Crystalline $Na_3V_2(PO_4)_3$ for Enhanced Sodium-Ion Storage. *Angew Chem Int Ed* **2021**, *60* (18), 10334−10341.
(150) Li, H.; Wu, C.; Bai, Y.; Wu, F.; Wang, M. Controllable synthesis of high-rate and long cycle-life $Na_3V_2(PO_4)_3$ for sodium-ion batteries. *J. Power Sources* **2016**, *326*, 14−22.
(151) Wang, Q.; Zhao, B.; Zhang, S.; Gao, X.; Deng, C. Superior sodium intercalation of honeycomb-structured hierarchical porous $Na_3V_2(PO_4)_3$/C microballs prepared by a facile one-pot synthesis. *Journal of Materials Chemistry A* **2015**, *3* (15), 7732−7740.
(152) Karthik, M.; Sathishkumar, S.; BoopathiRaja, R.; Meganathan, K. L.; Sumathi, T. Design and fabrication of $NaFePO_4$/MWCNTs hybrid electrode material for sodium-ion battery. *Journal of Materials Science: Materials in Electronics* **2020**, *31* (23), 21792−21801.
(153) Liu, Q.; Hu, Z.; Li, W.; Zou, C.; Jin, H.; Wang, S.; Chou, S.; Dou, S.-X. Sodium transition metal oxides: the preferred cathode choice for future sodium-ion batteries? *Energy Environ. Sci.* **2021**, *14* (1), 158−179.
(154) Dong, Y.; Feng, Y.; Deng, J.; He, P.; Ma, J. J. C. C. Electrospun Sb_2Se_3@C nanofibers with excellent lithium storage properties. *Chinese Chemical Letters* **2020**, *31* (3), 909−914. Li, H.; Xu, M.; Zhang, Z.; Lai, Y.; Ma, J. J. A. F. M. Engineering of polyanion type cathode materials for sodium-ion batteries: toward higher energy/power density. *Adv Funct Materials* **2020**, *30* (28), 2000473.
(155) Deng, C.; Zhang, S. 1D Nanostructured $Na_7V_4(P_2O_7)_4(PO_4)$ as High-Potential and Superior-Performance Cathode Material for Sodium-Ion Batteries. *ACS Appl. Mater. Interfaces* **2014**, *6* (12), 9111−9117.
(156) Chao, D.; Lai, C.-H. M.; Liang, P.; Wei, Q.; Wang, Y.-S.; Zhu, C. R.; Deng, G.; Doan-Nguyen, V. V. T.; Lin, J.; Mai, L.; Fan, H. J.; Dunn, B.; Shen, Z. X. Sodium Vanadium Fluorophosphates (NVOPF) Array Cathode Designed for High-Rate Full Sodium Ion Storage Device. *Advanced Energy Materials* **2018**, *8* (16), No. 1800058.

https://doi.org/10.1021/acsomega.4c02709
ACS Omega 2024, 9, 22509−22531

(157) Qi, Y.; Mu, L.; Zhao, J.; Hu, Y.-S.; Liu, H.; Dai, S. Superior Na-Storage Performance of Low-Temperature-Synthesized $Na_3(VO_{1-x}PO_4)_2F_{1+2x}$ ($0 \le x \le 1$) Nanoparticles for Na-Ion Batteries. *Angew Chem Int Ed* **2015**, *54* (34), 9911−9916.
(158) Li, C.; Shen, M.; Hu, B.; Lou, X.; Zhang, X.; Tong, W.; Hu, B. High-energy nanostructured $Na_3V_2(PO_4)_2O_{1.6}F_{1.4}$ cathodes for sodium-ion batteries and a new insight into their redox chemistry. *Journal of Materials Chemistry A* **2018**, *6* (18), 8340−8348.
(159) Xiang, X.; Lu, Q.; Han, M.; Chen, J. Superior high-rate capability of $Na_3(VO_{0.5})_2(PO_4)_2F_2$ nanoparticles embedded in porous graphene through the pseudocapacitive effect. *Chem. Commun.* **2016**, *52* (18), 3653−3656.
(160) Zhou, Q.; Wang, L.; Li, W.; Zhao, K.; Liu, M.; Wu, Q.; Yang, Y.; He, G.; Parkin, I. P.; Shearing, P. R.; et al. Sodium Superionic Conductors (NASICONs) as Cathode Materials for Sodium-Ion Batteries. *Electrochemical Energy Reviews* **2021**, *4* (4), 793−823.
(161) Zhu, Q.; Chang, X.; Sun, N.; Chen, R.; Zhao, Y.; Xu, B.; Wu, F. Confined Growth of Nano-$Na_3V_2(PO_4)_3$ in Porous Carbon Framework for High-Rate Na-Ion Storage. *ACS Appl. Mater. Interfaces* **2019**, *11* (3), 3107−3115.
(162) Li, J.-Y.; Zhao, Q.-Y.; Lin, X.-T.; Li, X.-D.; Sheng, H.; Liang, J.-Y.; Wu, X.-W.; Yin, Y.-X.; Guo, Y.-G.; Zeng, X.-X. A dynamic polyanion framework with anion/cation co-doping for robust Na/Zn-ion batteries. *J. Power Sources* **2022**, *530*, No. 231257.
(163) Das, A.; Majumder, S. B.; Roy Chaudhuri, A. K^+ and Mg^{2+} co-doped bipolar $Na_3V_2(PO_4)_3$: An ultrafast electrode for symmetric sodium ion full cell. *J. Power Sources* **2020**, *461*, No. 228149.
(164) Chen, R.; Butenko, D. S.; Li, S.; Li, D.; Zhang, X.; Cao, J.; Ogorodnyk, I. V.; Klyui, N. I.; Han, W.; Zatovsky, I. V. Effects of low doping on the improvement of cathode materials $Na_{3+x}V_{2-x}M_x(PO_4)_3$ (M = Co^{2+}, Cu^{2+}; x = 0.01−0.05) for SIBs. *Journal of Materials Chemistry A* **2021**, *9* (32), 17380−17389.
(165) Huang, Y.; Li, X.; Wang, J.; Miao, L.; Li, C.; Han, J.; Huang, Y. Superior Na-ion storage achieved by Ti substitution in $Na_3V_2(PO_4)_3$. *Energy Storage Materials* **2018**, *15*, 108−115.
(166) Klee, R.; Lavela, P.; Aragón, M. J.; Alcántara, R.; Tirado, J. L. Enhanced high-rate performance of manganese substituted $Na_3V_2(PO_4)_3$/C as cathode for sodium-ion batteries. *J. Power Sources* **2016**, *313*, 73−80.
(167) Chen, Y.; Xu, Y.; Sun, X.; Wang, C. Effect of Al substitution on the enhanced electrochemical performance and strong structure stability of $Na_3V_2(PO_4)_3$/C composite cathode for sodium-ion batteries. *J. Power Sources* **2018**, *375*, 82−92.
(168) Cheng, J.; Chen, Y.; Wang, Y.; Wang, C.; He, Z.; Li, D.; Guo, L. Insights into the enhanced sodium storage property and kinetics based on the Zr/Si codoped $Na_3V_2(PO_4)_3$/C cathode with superior rate capability and long lifespan. *J. Power Sources* **2020**, *474*, No. 228632.
(169) Chen, Y.; Xu, Y.; Sun, X.; Zhang, B.; He, S.; Wang, C. F-doping and V-defect synergetic effects on $Na_3V_2(PO_4)_3$/C composite: A promising cathode with high ionic conductivity for sodium ion batteries. *J. Power Sources* **2018**, *397*, 307−317.
(170) Zheng, Q.; Yi, H.; Liu, W.; Li, X.; Zhang, H. Improving the electrochemical performance of $Na_3V_2(PO_4)_3$ cathode in sodium ion batteries through Ce/V substitution based on rational design and synthesis optimization. *Electrochim. Acta* **2017**, *238*, 288−297.
(171) Liang, X.; Ou, X.; Zheng, F.; Pan, Q.; Xiong, X.; Hu, R.; Yang, C.; Liu, M. Surface Modification of $Na_3V_2(PO_4)_3$ by Nitrogen and Sulfur Dual-Doped Carbon Layer with Advanced Sodium Storage Property. *ACS Appl. Mater. Interfaces* **2017**, *9* (15), 13151−13162.
(172) Liang, L.; Li, X.; Zhao, F.; Zhang, J.; Liu, Y.; Hou, L.; Yuan, C. Construction and Operating Mechanism of High-Rate Mo-Doped $Na_3V_2(PO_4)_3$@C Nanowires toward Practicable Wide-Temperature-Tolerance Na-Ion and Hybrid Li/Na-Ion Batteries. *Advanced Energy Materials* **2021**, *11* (21), No. 2100287.
(173) Sun, S.; Chen, Y.; Cheng, J.; Tian, Z.; Wang, C.; Wu, G.; Liu, C.; Wang, Y.; Guo, L. Constructing dimensional gradient structure of $Na_3V_2(PO_4)_3$/C@CNTs-WC by wolfram substitution for superior sodium storage. *Chemical Engineering Journal* **2021**, *420*, No. 130453.
(174) Chen, Y.; Cheng, J.; Wang, C.; He, Z.; Wang, Y.; Li, D.; Guo, L. Simultaneous modified $Na_{2.9}V_{1.9}Zr_{0.1}(PO_4)_3$/C@rGO as a superior high rate and ultralong lifespan cathode for symmetric sodium ion batteries. *Chemical Engineering Journal* **2021**, *413*, No. 127451.
(175) Cao, Y.; Liu, Y.; Zhao, D.; Zhang, J.; Xia, X.; Chen, T.; Zhang, L.-c.; Qin, P.; Xia, Y. K-doped $Na_3Fe_2(PO_4)_3$ cathode materials with high-stable structure for sodium-ion stored energy battery. *J. Alloys Compd.* **2019**, *784*, 939−946.
(176) Guo, C.; Yang, J.; Cui, Z.; Qi, S.; Peng, Q.; Sun, W.; Lv, L.-P.; Xu, Y.; Wang, Y.; Chen, S. In-situ structural evolution analysis of Zr-doped $Na_3V_2(PO_4)_2F_3$ coated by N-doped carbon layer as high-performance cathode for sodium-ion batteries. *Journal of Energy Chemistry* **2022**, *65*, 514−523.
(177) Yi, H.; Ling, M.; Xu, W.; Li, X.; Zheng, Q.; Zhang, H. VSC-doping and VSU-doping of $Na_3V_{2-x}Ti_x(PO_4)_2F_3$ compounds for sodium ion battery cathodes: Analysis of electrochemical performance and kinetic properties. *Nano Energy* **2018**, *47*, 340−352.
(178) Liu, W.; Yi, H.; Zheng, Q.; Li, X.; Zhang, H. Y-Doped $Na_3V_2(PO_4)_2F_3$ compounds for sodium ion battery cathodes: electrochemical performance and analysis of kinetic properties. *Journal of Materials Chemistry A* **2017**, *5* (22), 10928−10935.
(179) Lv, Z.; Ling, M.; Yi, H.; Zhang, H.; Zheng, Q.; Li, X. Electrode Design for High-Performance Sodium-Ion Batteries: Coupling Nanorod-Assembled $Na_3V_2(PO_4)_3$@C Microspheres with a 3D Conductive Charge Transport Network. *ACS Appl. Mater. Interfaces* **2020**, *12* (12), 13869−13877.
(180) Jin, T.; Liu, Y.; Li, Y.; Cao, K.; Wang, X.; Jiao, L. Electrospun $NaVPO_4F$/C Nanofibers as Self-Standing Cathode Material for Ultralong Cycle Life Na-Ion Batteries. *Advanced Energy Materials* **2017**, *7* (15), No. 1700087.
(181) Ou, J.; Wang, H.; Deng, H.; Li, B.; Zhang, H. Hydrothermally prepared composite of $Na_3V_2(PO_4)_2F_3$ with gelatin and graphene used as a high-performance sodium ion battery cathode. *J. Alloys Compd.* **2022**, *926*, No. 166857.
(182) Liu, S.; Wang, L.; Liu, J.; Zhou, M.; Nian, Q.; Feng, Y.; Tao, Z.; Shao, L. $Na_3V_2(PO_4)_2F_3$−SWCNT: a high voltage cathode for non-aqueous and aqueous sodium-ion batteries. *Journal of Materials Chemistry A* **2019**, *7* (1), 248−256.
(183) Li, X.; Wang, S.; Tang, X.; Zang, R.; Li, P.; Li, P.; Man, Z.; Li, C.; Liu, S.; Wu, Y.; et al. Porous $Na_3V_2(PO_4)_3$/C nanoplates for high-performance sodium storage. *J. Colloid Interface Sci.* **2019**, *539*, 168−174.
(184) Zheng, Q.; Ni, X.; Lin, L.; Yi, H.; Han, X.; Li, X.; Bao, X.; Zhang, H. Towards enhanced sodium storage by investigation of the Li ion doping and rearrangement mechanism in $Na_3V_2(PO_4)_3$ for sodium ion batteries. *Journal of Materials Chemistry A* **2018**, *6* (9), 4209−4218.
(185) Xiao, L.; Ji, F.; Zhang, J.; Chen, X.; Fang, Y. J. S. Doping Regulation in Polyanionic Compounds for Advanced Sodium-Ion Batteries. *Small* **2023**, *19* (1), 2205732.
(186) Li, L.; Liu, X.; Tang, L.; Liu, H.; Wang, Y.-G. Improved electrochemical performance of high voltage cathode $Na_3V_2(PO_4)_2F_3$ for Na-ion batteries through potassium doping. *J. Alloys Compd.* **2019**, *790*, 203−211.
(187) Li, H.; Yu, X.; Bai, Y.; Wu, F.; Wu, C.; Liu, L.-Y.; Yang, X.-Q. Effects of Mg doping on the remarkably enhanced electrochemical performance of $Na_3V_2(PO_4)_3$ cathode materials for sodium ion batteries. *J. Mater. Chem. A* **2015**, *3* (18), 9578−9586.
(188) Zhao, L.; Zhao, H.; Du, Z.; Wang, J.; Long, X.; Li, Z.; Swierczek, K. Delicate lattice modulation enables superior Na storage performance of $Na_3V_2(PO_4)_3$ as both an anode and cathode material for sodium-ion batteries: understanding the role of calcium substitution for vanadium. *J. Mater. Chem. A* **2019**, *7* (16), 9807−9814.
(189) Liu, J.; Zhang, L.-L.; Cao, X.-Z.; Lin, X.; Shen, Y.; Zhang, P.; Wei, C.; Huang, Y.-Y.; Luo, W.; Yang, X.-L. Achieving the Stable Structure and Superior Performance of $Na_3V_2(PO_4)_2O_2F$ Cathodes via Na-Site Regulation. *ACS Applied Energy Materials* **2020**, *3* (8), 7649−7658.
(190) Li, S.-F.; Gu, Z.-Y.; Guo, J.-Z.; Hou, X.-K.; Yang, X.; Zhao, B.; Wu, X.-L. Enhanced electrode kinetics and electrochemical properties

https://doi.org/10.1021/acsomega.4c02709
ACS Omega 2024, 9, 22509−22531

of low-cost $NaFe_2PO_4(SO_4)_2$ via Ca^{2+} doping as cathode material for sodium-ion batteries. *Journal of Materials Science & Technology* **2021**, *78*, 176−182.
(191) Puspitasari, D. A.; Patra, J.; Hernandha, R. F. H.; Chiang, Y.-S.; Inoishi, A.; Chang, B. K.; Lee, T.-C.; Chang, J.-K. J. A. A. M. Enhanced Electrochemical Performance of Ca-Doped $Na_3V_2(PO_4)_2F_3$/C Cathode Materials for Sodium-Ion Batteries. *ACS Appl. Mater. Interfaces* **2024**, *16* (1), 496−506.
(192) Aragón, M. J.; Lavela, P.; Ortiz, G. F.; Tirado, J. L. Benefits of Chromium Substitution in $Na_3V_2(PO_4)_3$ as a Potential Candidate for Sodium-Ion Batteries. *ChemElectroChem* **2015**, *2* (7), 995−1002.
(193) Zhang, Y.; Guo, S.; Xu, H. Synthesis of uniform hierarchical $Na_3V_{1.95}Mn_{0.05}(PO_4)_2F_3$@C hollow microspheres as a cathode material for sodium-ion batteries. *Journal of Materials Chemistry A* **2018**, *6* (10), 4525−4534.
(194) Zhao, L.; Zhao, H.; Du, Z.; Wang, J.; Long, X.; Li, Z.; Świerczek, K. Delicate lattice modulation enables superior Na storage performance of $Na_3V_2(PO_4)_3$ as both an anode and cathode material for sodium-ion batteries: understanding the role of calcium substitution for vanadium. *Journal of Materials Chemistry A* **2019**, *7* (16), 9807−9814.
(195) Li, H.; Yu, X.; Bai, Y.; Wu, F.; Wu, C.; Liu, L.-Y.; Yang, X.-Q. Effects of Mg doping on the remarkably enhanced electrochemical performance of $Na_3V_2(PO_4)_3$ cathode materials for sodium ion batteries. *Journal of Materials Chemistry A* **2015**, *3* (18), 9578−9586.
(196) Zhao, X.-X.; Fu, W.; Zhang, H.-X.; Guo, J.-Z.; Gu, Z.-Y.; Wang, X.-T.; Yang, J.-L.; Lü, H.-Y.; Wu, X.-L.; Ang, E. H. Pearl-Structure-Enhanced NASICON Cathode toward Ultrastable Sodium-Ion Batteries. *Advanced Science* **2023**, *10* (19), No. 2301308.
(197) Zhang, D.; Feng, P.; Xu, B.; Li, Z.; Qiao, J.; Zhou, J.; Chang, C. High Rate Performance of $Na_3V_{2-x}Cu_x(PO_4)_3$/C Cathodes for Sodium Ion Batteries. *J. Electrochem. Soc.* **2017**, *164* (14), A3563.
(198) Jin, D.; Qiu, H.; Du, F.; Wei, Y.; Meng, X. Co-doped Na_2FePO_4F fluorophosphates as a promising cathode material for rechargeable sodium-ion batteries. *Solid State Sci.* **2019**, *93*, 62−69.
(199) Liu, X.; Tang, L.; Li, Z.; Zhang, J.; Xu, Q.; Liu, H.; Wang, Y.; Xia, Y.; Cao, Y.; Ai, X. An Al-doped high voltage cathode of $Na_4Co_3(PO_4)_2P_2O_7$ enabling highly stable 4 V full sodium-ion batteries. *Journal of Materials Chemistry A* **2019**, *7* (32), 18940−18949.
(200) Chen, M.; Hua, W.; Xiao, J.; Zhang, J.; Lau, V. W.-h.; Park, M.; Lee, G.-H.; Lee, S.; Wang, W.; Peng, J.; et al. Activating a Multielectron Reaction of NASICON-Structured Cathodes toward High Energy Density for Sodium-Ion Batteries. *J. Am. Chem. Soc.* **2021**, *143* (43), 18091−18102.
(201) Li, P.; Gao, M.; Wang, D.; Li, Z.; Liu, Y.; Liu, X.; Li, H.; Sun, Y.; Liu, Y.; Niu, X.; Zhong, B.; Wu, Z.-G.; Guo, X. Optimizing vanadium redox reaction in $Na_3V_2(PO_4)_3$ cathodes for sodium-ion batteries by the synergistic effect of additional electrons from heteroatoms. *ACS Appl. Mater. Interfaces* **2023**, *15* (7), 9475−9485.
(202) Chen, M.; Hua, W.; Xiao, J.; Zhang, J.; Lau, V. W.-h.; Park, M.; Lee, G.-H.; Lee, S.; Wang, W.; Peng, J.; Fang, L.; Zhou, L.; Chang, C.-K.; Yamauchi, Y.; Chou, S.; Kang, Y.-M. Activating a multielectron reaction of NASICON-structured cathodes toward high energy density for sodium-ion batteries. *J. Am. Chem. Soc.* **2021**, *143* (43), 18091−18102.
(203) Park, J. Y.; Shim, Y.; Kim, Y.-i.; Choi, Y.; Lee, H. J.; Park, J.; Wang, J. E.; Lee, Y.; Chang, J. H.; Yim, K.; et al. An iron-doped NASICON type sodium ion battery cathode for enhanced sodium storage performance and its full cell applications. *Journal of Materials Chemistry A* **2020**, *8* (39), 20436−20445.
(204) Zhan, R.; Shen, B.; Xu, Q.; Zhang, Y.; Luo, Y.; Liu, H.; Chen, H.; Liu, F.; Li, C.; Xu, M. Half-cell and full-cell applications of sodium ion batteries based on carbon-coated $Na3Fe_{0.5}V_{1.5}(PO_4)_3$ nanoparticles cathode. *Electrochim. Acta* **2018**, *283*, 1475−1481.
(205) Liu, M.; Li, M.; Zhang, B.; Li, H.; Liang, J.; Hu, X.; Liu, H.; Ma, Z.-F. Anionic Group Doping of $Na_4Fe_3(PO_4)_2P_2O_7$ Stabilizes Its Structure and Improves Electrochemical Performance for Sodium Ion Storage. *ACS Sustainable Chem. Eng.* **2023**, *11* (51), 18102−18111.

https://doi.org/10.1021/acsomega.4c02709
ACS Omega 2024, 9, 22509−22531